Upper ocean temperature characteristics in the subantarctic Southeast Pacific based on biomarker reconstructions

Julia R. Hagemann[1], Lester Lembke-Jene[1], Frank Lamy[1], Maria-Elena Vorrath[2], Jérôme Kaiser[3], Juliane Müller[1], Helge W. Arz[3], Jens Hefter[1], Andrea Jaeschke[4], Nicoletta Ruggieri[1], Ralf Tiedemann[1]

5 [1]Alfred Wegener Institute, Helmholtz Centre for Polar and Marine Research, 27570 Bremerhaven, Germany
[2]Institute for Geology, University Hamburg, 20146 Hamburg, Germany
[3]Leibniz-Institute for Baltic Sea Research Warnemünde, 18119 Rostock, Germany
[4]Institute of Geology and Mineralogy, University of Cologne, 50923 Cologne, Germany

10 *Correspondence to*: Julia. R. Hagemann (Julia.Hagemann@awi.de) and Lester Lembke-Jene (Lester.Lembke-Jene@awi.de)

Abstract. Alkenones and Glycerol Dialkyl Glycerol Tetraether lipids (GDGT) as remnants of living organisms are widely used biomarkers for determining past oceans' water temperatures. The organisms these proxy carriers stem from, are influenced by a number of environmental parameters, such as water depth, nutrient availability, light conditions or seasonality, which all may significantly bias the calibration to ambient water temperatures. Reliable temperature determinations remain

15 thus challenging, especially in higher latitudes and for under-sampled regions. We analyzed 33 sediment surface samples from the Southern Chilean continental margin and the Drake Passage for alkenones and GDGTs and compared the results with gridded instrumental reference data from the World Ocean Atlas 2005 (WOA05), as well as previously published data from an extended study area covering the Central and Western South Pacific towards the New Zealand continental margin. We show that for alkenone-derived SSTs, the widely-used global core-top calibration of Müller et al. (1998) yields the smallest residuals,

20 whereas the calibration of Sikes et al. (1997), adapted to higher latitudes and supposed to show summer SSTs, overestimates modern WOA05-based (summer and annual mean) SSTs. Our alkenone SSTs show a slight seasonal shift of ~1° C at the Southern Chilean Margin and up to ~2° C in the Drake Passage towards austral summer SSTs, whereas samples in the Central South Pacific reflect an annual mean signal. We show that for GDGT-based temperatures, a more complex pattern emerges. In areas north of the Subantarctic Front (SAF) the subsurface calibration of Kim et al. (2012a) best reflects temperatures from

25 the WOA05, largely within the margin error of ±2.2° C. Temperatures south of the SAF instead are significantly overestimated by up to 14° C, irrespective of the applied calibration. Based on a qualitative assessment of the GDGT [2]/[3]-ratios, which likely indicate water depth of origin, our samples reflect a subsurface (0 to 200 m water depth) rather than a surface (0 – 50 m water depth) signal. The overestimation of surface and subsurface temperatures south of the SAF highlights the need for a re-assessment of existing calibrations in the polar Southern Ocean, and leads to limitations in reliably both obtaining absolute

30 values and assessing relative changes. Therefore, we suggest a modified Southern Ocean calibration for surface and subsurface GDGT-based temperatures, which shows a lower temperature sensitivity of the TEX^L_{86} and yields principally lower absolute temperatures, which align more closely with WOA05-derived values.

1 Introduction

Alkenones and GDGTs (Glycerol Dialkyl Glycerol Tetraether; Schouten et al., 2002) are widely used for determining oceans'
35 past water temperatures. These biomarkers are present in all oceans and occur from the tropics to high latitudes (e.g., Herbert
et al., 2010; Sikes et al., 1997). Alkenone-derived sea surface temperatures (SSTs) are based on lipid remains of
photoautotrophic Coccolithophorids (e.g., Baumann et al., 2005). The ratio of di- and tri-unsaturated alkenones, expressed as
the Unsaturation Ketone index $U^{K'}_{37}$ (**Table A1**) is reflecting SSTs (Prahl and Wakeham, 1987). Calculation of SSTs is based
on calibration equations developed over the past ~40 years (**Table A1**). Most of these empirically-derived equations are
40 relatively similar, based on either culture experiments (Prahl et al., 1988; Prahl and Wakeham, 1987) or surface sediment
samples from tropical to subpolar regions with corresponding instrumental data (Müller et al., 1998). Other calibrations (e.g.,
Sikes et al., 1997) were developed specifically for (sub)polar regions and are adapted for a seasonal bias toward summer SSTs.
In the following, we use the terms Müller98 for the calibration by Müller et al. (1998) and Sikes97 for the calibration by Sikes
et al. (1997; **Table A1**).

45   The accuracy of Alkenone-based calibrations can be influenced by other environmental factors besides temperature, such
as light levels, changes in growth rate or nutrient availability. None of these factors seems to have an appreciable effect on the
$U^{K'}_{37}$ index (e.g., Caniupán et al., 2014; Epstein et al., 2001; Herbert, 2001; Popp et al., 1998). In contrast, preferential
degradation of the alkenone $C_{37:3}$ in sediment under aerobic conditions may bias the $U^{K'}_{37}$ signal towards warmer SSTs (Prahl
et al., 2010). However, seasonality often plays a significant role in higher latitudes (e.g., Max et al., 2020; Prahl et al., 2010),
50 due to primary production being more pronounced in the thermal summer season combined with the principally wider spread
in temperatures across the seasonal cycle. In the case of our study region, samples from the Central South Pacific are most
likely to represent either summer temperatures (with the Sikes97 calibration) or an annual mean (Müller98 calibration;
Jaeschke et al., 2017). Prahl et al. (2010) instead, using samples from the Chilean continental slope, found a slight seasonal
summer bias south of ~50° S. In addition, studies from the North Pacific show that alkenone temperatures in higher latitudes
55 differ from the annual mean by up to 6° C, recording late summer to autumn SSTs instead (e.g., Max et al., 2020; Prahl et al.,
2010).

In addition to the alkenone-derived paleo-thermometer, other biomarkers also bear considerable and well-established
potential to reconstruct past temperatures. GDGTs are lipid remains of *Thaumarchaeota* (formerly called Crearchaeota Group
I; Brochier-Armanet et al., 2008) and contain zero to four cyclopentane moieties in their molecule structure (GDGT-0; GDGT-
60 1; GDGT-2; GDGT-3; Crenarchaeol), whereas Crenarchaeol and its isomer Cren' feature four cyclopentane and one hexane
moieties. The number of moieties increases with growth temperature (Schouten et al., 2002). Determination of GDGT-derived
water temperatures is based on the Tetraether index (TEX86; Schouten et al., 2002), or their modifications TEX^{H}_{86} and TEX^{L}_{86}
(**Table A1**), which have been determined for water temperatures >15° C and <15° C, respectively (Kim et al., 2010). While
TEX^{H}_{86} is a logarithmic function of the original index, TEX^{L}_{86} deletes the GDGT-3 from the denominator and removes the
65 isomer Cren' from the equation, due to a weaker correlation to water temperatures in cold regions (Kim et al., 2010). In contrast

to photo-autotrophic coccolithophores, *Thaumarchaeota* occur throughout the water column (Karner et al., 2001), which complicates the attribution of the recorded temperature signal to specific water depths. In general, it is assumed that *Thaumarchaeota* predominantly reflect either a subsurface, i.e., seasonal mixed-layer temperature (Tsub; 0 – 200 m water depth), or an SST signal (**Table A1**), because the grazing and repacking of GDGTs into fecal pellets occurs most effectively

70   within the photic zone (Wuchter et al., 2005). The GDGT [2]/[3]-ratio can be used to qualitatively determine the habitat depth of the *Thaumarchaeota*, since it increases with increasing water depth (Dong et al., 2019; Hernández-Sánchez et al., 2014; Kim et al., 2015; Kim et al., 2016; Schouten et al., 2012; Taylor et al., 2013). For the subpolar and polar Southern Ocean, in particular the extensive SE Pacific sector, only little information exists to date about the applicability of those different temperature proxies and their respective calibrations. In addition, systematic comparisons between alkenone and GDGT-based

75   temperature reconstructions based on surface sediments have thus far been limited (Jaeschke et al., 2017; Kaiser et al., 2015). In the following, we use the terms $SST^H Kim$ and $SST^L Kim$ for the two global surface calibrations by Kim et al. (2010), $Tsub^H Kim$ and $Tsub^L Kim$ for the two global subsurface calibrations by Kim et al. (2012a, 2012b) and $SST^H Kaiser$ and $Tsub^H Kaiser$ for the local surface and subsurface calibration by Kaiser et al. (2015; **Table A1**).

In this study, we present a new set of 33 sediment surface samples located along the Southern Chilean Margin (SCM) and

80   the Drake Passage (DP; ~52 – 62° S) to determine upper ocean water temperatures based on alkenones ($U^{K'}_{37}$) and GDGTs (TEX^H_{86} and TEX^L_{86}). We compare our regional results with previously published data from an extended, temperate to subpolar South Pacific study area (**Figure 1**).

We assess the applicability of the Müller98 and Sikes97 calibrations with World Ocean Atlas (WOA05)-based temperatures and investigate the influence of seasonality on alkenone-based temperature reconstructions. Furthermore, we compare the

85   GDGT-based indices TEX^H_{86} and TEX^L_{86} and their most common calibrations for SST and Tsub (**Table A1**) with World Ocean Atlas (WOA05)-based temperatures. Lastly, we check the potential influence of habitat depth on signal incorporation on the basis of the GDGT [2]/[3]-ratio and propose a new calibration specifically for the polar Pacific sector of the Southern Ocean (SO) south of the Subantarctic Front.

2 Study Area

90   Our study area comprises the subpolar and polar SE Pacific sector of the SO, including the Drake Passage. One important characteristic of the SO is the eastward-flowing Antarctic Circumpolar Current (ACC), which is largely driven by Southern Westerly Winds (SWW) and buoyancy forcing (Rintoul, 2018; Watson et al., 2015). The ACC flows unimpeded around Antarctica, and is only slowed down by the South American continent (Orsi et al., 1995), where the northern branch of the ACC bifurcates at ~40 – 45° S into the northward-flowing Peru-Chile Current (PCC) and the southward-flowing Cape Horn

95   Current (CHC; Strub et al., 1998). CHC and ACC jointly transport ca. 130 – 150 Sv of water (e.g., Koenig et al., 2014) through the ~800 km wide Drake Passage into the Atlantic Ocean (**Figure 1**).

Several fronts within the ACC characterize the convergence of water masses that differ in temperature, salinity and nutrient content (Orsi et al., 1995). The northern boundary of the ACC is defined by the Subtropical Front (STF; Orsi et al., 1995), followed from north to south by the Subantarctic Front (SAF), the Polar Front (PF) and the Southern ACC Front (SACCF).

100 Apart from the STF, which is interrupted by the South American continent, all three fronts (SAF, PF and SACCF) pass through the Drake Passage (Orsi et al., 1995). The zones between the fronts are defined as areas with differing temperature and salinity characteristics, both decreasing with increasing latitude. The SAF marks the beginning of the Antarctic Intermediate Water's (AAIW) northward descent to a depth of ~500 m. AAIW itself is associated with a salinity minimum of <34 PSU. The PF, on the other hand, marks the northern temperature limit of the cold Antarctic surface water. The SACCF instead has no distinct

105 separating features in the surface water. The boundary here is defined along the mesopelagic temperature maximum of the upwelled Upper Circumpolar Deep Water (UCDW; Orsi et al., 1995 and references therein).

3 Material and Methods

A total amount of 33 Multi-Corer (MUC) samples (**Table A2**) along the Southern Chilean Margin and the Drake Passage were analyzed for alkenones and GDGTs. The samples were collected during R/V Polarstern PS97 in February-April 2016 (Lamy,

110 2016) along a latitudinal transect on the Southern Chilean Margin and through the Southern Ocean frontal system.

The MUC samples were stored deep-frozen immediately onboard and freeze-dried afterwards in the laboratory. Extraction of the biomarkers was carried out with two different approaches. Between 3 and 5 g of ground surface sediment (0 – 1 cm) from each site was extracted either by an accelerated Solvent Extraction (DIONEX ASE 350; Thermo Scientific) with DCM:MeOH (9:1, v:v) or in an ultrasonic bath with DCM:MeOH (2:1, v:v). The bulk of the solvent was removed by rotary

115 evaporation, under a nitrogen gas stream or in a Rocket Evaporator (Genevac – SP Scientific). The different fractions were chromatographically separated using small glass columns filled with 5 cm of activated silicagel. After adding the sample, the column was rinsed with 5 ml n-hexane, 5 ml or 8 ml n-hexane:DCM (1:1, v:v), 5 ml DCM and 4 ml DCM:MeOH (1:1, v:v) to yield n-alkanes, alkenones and GDGTs, respectively. The samples were dried again and transferred into 2 ml vials. As internal standard, 100 µl each of the n-alkane C_{36} or 2-nonadecanone standard and C_{46} were added before extraction. For the

120 measurement, the alkenone fractions were diluted with 200 – 20 µl n-hexane, the GDGT fraction was diluted with 50 – 120 µl n-hexane:isopropanol (1%).

Alkenones were injected with 1 µl solvent and Helium as carrier gas into an Agilent HP6890 Gas Chromatograph equipped with a 60 m DB-1 MS column and a flame ionization detector. The oven temperature was increased from initially 60° C to 150° C with 20° C min^{-1} and thereafter with 6° C min^{-1} until 320° C were reached.

125 For the GDGT extraction of most of the samples of the Drake Passage see Lamping et al. (2021) and Vorrath et al. (2020). The other part of the GDGT samples were analyzed on an Agilent 1260 Infinity II ultrahigh-performance liquid chromatography-mass spectrometry (UHPLC-MS) system and a G6125C single quadrupole mass spectrometer. The chromatographic separation was achieved by coupling two UPLC silica columns (Waters Acquity BEH HILIC, 2.1 × 150 mm,

1.7 μm) and a 2.1 × 5 mm pre-column as in Hopmans et al. (2016), but with the following chromatographic modifications:
130 Mobile phases A and B consisted of *n*-hexane: chloroform (99:1, v/v) and *n*-hexane: 2-propanol: chloroform (89:10:1, v/v/v), respectively. The flow rate was set to 0.4 ml/min and the columns heated to 50°C, resulting in a maximum backpressure of 425 bar. Sample aliquots of 20 μl were injected with isocratic elution for 20 minutes using 86% A and 14% B, followed by a gradient to 30% A and 70% B within the next 20 min. After this, the mobile phase was set to 100% B and the column rinsed for 13 min, followed by 7 min re-equilibration time with 86% A and 14% B before the next sample analysis. The total run time
135 was 60 min.

GDGTs were detected using positive ion APCI-MS and selective ion monitoring (SIM) of $(M + H)^+$ ions (Schouten et al., 2007) with the following settings: nebulizer pressure 50 psi, vaporizer and drying gas temperature 350°C, drying gas flow 5 L/min. The capillary voltage was 4 kV and the corona current +5 μA. The detector was set for the following SIM ions: *m/z* 744 (C_{46} standard), *m/z* 1302.3 (GDGT-0), *m/z* 1300.3 (GDGT-1), *m/z* 1298.3 (GDGT-2), *m/z* 1296.3 (GDGT-3), *m/z* 1292.3
140 (Crenarchaeol and Cren' isomer). The resulting scan/dwell time was 66 ms.

4 Results and Discussion

On our meridional transect along the Chilean margin, $U^{K'}_{37}$ values range from 0.07 (PS97/079) to 0.38 (PS97/132), with minimum values in the southernmost region and increasing values to the north. All indices from alkenones and GDGTs are listed in **Table A2**. In the following, we compare the two most widely used calibrations for alkenones in this region: the
145 subpolar and polar SO Sikes97 calibration, as well as the Müller98 calibration.

4.1 Alkenone-based Sea Surface Temperatures

Alkenone-based SSTs calculated with Müller98 range from ~10° C in the northernmost locations of our study area to ~1° C in the southern part of the Drake Passage, south of the PF (**Figure 2A, B**). SST estimates based on Sikes97 instead range from ~12.5° C in the northernmost locations to ~4° C in the Drake Passage (**Figure 2C, D**). Most values fit closely to the Müller98
150 calibration line of both, annual mean and summer SSTs, but show an offset to the Sikes97 calibration line (**Figure 3**). Although Sikes97 was specifically adapted to the subpolar and polar SO, it generally overestimates modern SSTs in this study area, both for annual mean and summer (**Figure 2** and **Figure 3**). Our samples for the SE Pacific fit well to Müller98, but not to Sikes97 (**Figure 2** and **Figure 3**). Because of the latter's overestimation of modern temperatures, we hereafter chose to solely use the Müller98 calibration.

4.2 Influence of seasonality on alkenone temperature reconstruction

4.2.1 Seasonal signal along the Chilean Margin

Our alkenone-based SSTs fits world ocean atlas-derived annual mean and summer temperatures, showing only a small seasonal effect towards warmer SSTs. This observation is also in line with previous data from the Northern – Central Chilean Margin,

160   which yields a slight seasonal effect south of 50° S (Prahl et al., 2006; Prahl et al., 2010). Also, a previous study from the Chilean fjord region confirms SST signals being only slightly shifted towards summer in the southern Chilean fjord region (Fig. 4; Caniupán et al., 2014). Along the Chilean continental margin, this seasonal summer effect even further decreases southward to only ~1° C (i.e., summer SSTs vs. annual mean) between 50 – 57° S, based on WOA05-derived SSTs (**Figure 4**; blue and yellow cross). This deviation of 1° C, at least north of the SAF, is within the generally accepted error range for alkenone-derived paleo-SSTs of ±1.5° C (Müller et al., 1998), so that seasonality here appears to be negligible. Only further

165   south in the Drake Passage, deviations of our reconstructed summer temperatures from the annual mean increase to about 2° C, which are likewise reflected in WOA05-based SSTs (**Figure 4**).

In addition, not all data uniformly show a seasonal trend. Our results reveal a rather localized structure that shows a general tendency towards a summer signal, except for two regions in our data set that reflect annual means instead (**Figure 4**; red circles). The first region is located between ~54 – 58° S near the Strait of Magellan, where Atlantic waters mix with Pacific

170   waters. The second region encompasses samples in the DP located close to the PF. The PF marks the temperature boundary of the cold Antarctic surface water, which is subducted at the PF and transported northwards (Orsi et al., 1995 - and references therein). This vertical water mass structure likely suppresses potential seasonal effects by providing homogenous temperatures throughout the annual cycle. The effects of the frontal system in the ACC on alkenone production is indicated by several studies based on coccolithophorids (e.g., Saavedra-Pellitero et al., 2014; Vollmar et al., 2022; Saavedra-Pellitero et al., 2019).

175   The coccolithophore assemblages between the PF and the SAF show a significantly reduced diversity compared to north of the SAF. South of the PF, coccolithophorids occur only sporadically and show a reduced diversity (Saavedra-Pellitero et al., 2014).

This weakly expressed seasonality in our results, which remains mostly within the error range of Müller98, is in stark contrast to results from other regions, notably the subarctic North Pacific. There, several studies showed a more consistent seasonal

180   shift towards summer and autumn SSTs of 4 – 6° C north of the subarctic front, while locations south of the subarctic front reflect an annual mean (Max et al., 2020; Méheust et al., 2013; Prahl et al., 2010). The subarctic front in the North Pacific acts as a natural boundary, essentially creating a highly stratified subarctic surface ocean with a permanent halocline. In contrast, the transition in the South Pacific from subtropical to polar regions is characterized by a lower salinity gradient and stratification, leading to a less pronounced SAF.

185   **4.2.2 Regional seasonality patterns across the South Pacific**

We compared the samples from our relatively small study region with published data from the South Pacific Gyre, the Central South Pacific, the New Zealand Margin (Jaeschke et al., 2017) and the Northern – Central Chilean Margin (Prahl et al., 2006; Prahl et al., 2010) based on the Müller98 and Sikes97 calibrations (**Figure 5**). We also calculated the residual temperatures by subtracting the modern WOA05 temperatures at 10 m water depth from our calculated temperatures, shown in combination

190   with $U^{K'}_{37}$ against SSTs (**Figure 5**). The Central South Pacific and New Zealand Margin samples of Jaeschke et al. (2017) spread over a wide area with different conditions. Taking into account a seasonal effect towards summer SSTs, only few

samples of this extended data set match with the Sikes97 calibration (Fig. 5A, B; Jaeschke et al., 2017). In contrast, the Müller98 calibration is applicable in the entire extended study area when compared with both, annual mean and summer SSTs, reaffirming our decision to use Müller98 for further analyses.

195   The SCM and the Drake Passage samples are generally warmer by ~1.5° C than the samples from the Central South Pacific region (**Figure 6**). The Central South Pacific samples represent a best fit to annual mean, in contrast to the SCM and DP samples, which have a slight, but mostly negligible, seasonal shift toward summer SSTs (**Figure 6**). This tendency to summer SSTs in the SE-Pacific could be due to several factors like changes in the current and wind regimes, or nutrient availability, leading to a potentially changing competition between different primary producers. Such higher nutrient availability during

200   the summer months might be amplified by the close proximity of the SE Pacific samples to South America, where high precipitation rates of 3,000 – 10,000 mm/yr reach their maximum in South Patagonia during the summer months (e.g., Garreaud et al., 2013; Lamy et al., 2010; Schneider et al., 2003). The increased precipitation during the summer months results in an increased freshwater runoff (e.g., Dávila et al., 2002) accompanied by increased supply of continent-derived nutrients to hemipelagic and Drake passage waters (Toyos et al., 2022). In addition, higher stratification by an increased freshwater supply

205   due to the proximity to the continental shelf could favor a seasonal coccolithophore bloom.

The area off New Zealand correlates well with samples off the Northern – Central Chilean Margin north of ~45° S and corresponds to the annual mean (**Figure 6**). In contrast, the South Pacific Gyre samples reflect a summer to autumn signal (Fig. 6; Jaeschke et al., 2017). These latter sample locations are characterized by an extremely low nutrient content and accordingly low primary production (D'hondt et al., 2009). Due to the pelagic setting distant from potential continental input

210   other than through dust, and with relatively deep thermocline settings, only little nutrient advection and upwelling occurs in this area (D'hondt et al., 2009; Lamy et al., 2014), as evidenced by low alkenones, *n*-alkanes and brGDGTs concentrations (Jaeschke et al., 2017). These factors likely lead to a seasonal bias if e.g., dust transport and macronutrient supply are increased in late spring to summer, but relatively quickly exhausted before a sustained alkenone production would record an annual mean temperature signal, due to the deep and stable thermocline inhibiting further macronutrient supply.

215   **4.3 GDGT – based (sub)surface temperatures**

Similar to $U^{K'}_{37}$ values, GDGT-derived indices TEX^{H}_{86} and TEX^{L}_{86} increase along our transect from south to north. The values range from –0.48 to –0.61 (PS97/079) and from –0.39 to –0.53 (PS97/131) for TEX^{H}_{86} and TEX^{L}_{86}, respectively (cf. **Table A2**). In contrast to Coccolithophorids, *Thaumarchaeota* live at greater water depths (e.g., Karner et al., 2001) and occur at higher latitudes (e.g., Massana et al., 1998; Murray et al., 1998), which complicates the choice of an adequate temperature

220   calibration, since reference data and sample sites for both characteristics remain scarce. For the GDGTs, we use six calibrations in total for both indices: the surface calibrations $SST^{H}Kim$, $SST^{H}Kaiser$ and $SST^{L}Kim$, as well as the subsurface calibrations $Tsub^{H}Kim$, $Tsub^{H}Kaiser$ and $Tsub^{L}Kim$ (**Table A1**).

Surface and subsurface ranges for GDGTs are following the definition of Kaiser et al. (2015), Kim et al. (2012b) and Kim et al. (2012a), with a mean of 0 – 50 m water depth and 0 – 200 m water depth, respectively. We therefore used the WOA05-

225 derived temperatures of depths from 10 m and 125 m for surface and subsurface, as they roughly correspond to the average values (**Figure 7**). Based on the surface calibrations, the temperatures range from ~11.5° C to 5° C for SST^{H}Kim, from ~9.5° C to 4° C for SST^{H}Kaiser, and from ~13° C to 6° C for SST^{L}Kim. With the subsurface calibrations, the temperatures range from ~9° C to 4° C for Tsub^{H}Kim, ~9° C to 5 for Tsub^{H}Kaiser, and from ~10° C to 5° C for Tsub^{L}Kim (**Figure 7**).

The locations north of the SAF fit best to the modern WOA05-derived SSTs with the SST^{H}Kaiser calibration (**Figure 7B**)
230 and appear to extend the surface regression line along the 5 – 10° C temperature range (**Figure 8A**). On average, the modern temperatures are overestimated by ~1.3° C, which means they are no longer within the ±0.8° C standard error determined by Kaiser et al. (2015) for the surface calibration. In the subsurface, the Tsub^{H}Kim and Tsub^{H}Kaiser calibrations equally fit the modern WOA05-derived Tsub (**Figure 7D, E**), but the samples tend to fit better with the calibration line of Tsub^{H}Kim (**Figure 8B**). On average, the modern WOA05-derived Tsub are overestimated here by ~1.6° C. Thus, the calculated temperatures are
235 within the of ±2.2° C error range given by Kim et al. (2012a), but not within the ±0.6° C given by Kaiser et al. (2015) for the subsurface calibration. The samples from the DP instead, do not fit to any calibration and overestimate modern WOA05-derived SSTs or Tsub in all calibrations (**Figure 7** and **Figure 8**).

Apart from absolute temperature values, the slope of the various calibrations provides the potential to calculate relative temperature changes in time series. To determine which calibration best captures relative temperature changes in our study
240 region, we compared our samples with published data from the Central South Pacific and New Zealand Margin (Ho et al., 2014; Jaeschke et al., 2017), in addition to the Northern – Central Chilean Margin (Kaiser et al., 2015) dataset (**Figure 9**). In **Figure 9A – D** we show in red the regressions of all sites located north of the SAF (called ''local regression'' hereafter) in comparison to the published six different SST and Tsub calibrations of both Kim et al. (2010, 2012a and b), and Kaiser et al. (2015). In addition, we show the residuals in **Figure 9E, F** to illustrate which data are within the error range of the respective
245 calibrations. For this purpose, the mean WOA05 values of 0 – 50 m and 0 – 200 m of the annual mean were subtracted from the respective temperature calibration.

The slope of the SST^{H}Kim calibration shows a difference of ~3.2 to our local regression (**Figure 9A**), and yields best the relative temperature change across the region north of the SAF, although it generally yields the highest residuals (**Figure 9E**). The Tsub^{H}Kim calibration, with a difference of ~3.9 between the two slopes (**Figure 9C**), captures the relative temperature
250 changes as well. The latter corresponds to a temperature change (TEX$^H_{86}$: -0.2 to -0.3) of 5.5° C with Tsub^{H}Kim and 5.1° C with our local regression. In contrast to SST^{H}Kim, the residuals are smaller and within the reported error range of ±2.2° C (Kim et al., 2012a) for most samples north of the SAF (**Figure 9F**). Again, the central South Pacific samples located south of the SAF significantly overestimate local SSTs or Tsub with annual residuals of ~8.4° C (SST^{H}Kim), ~6.6° C (SST^{H}Kaiser), ~8.1° C (SST^{L}Kim), ~6.4° C (Tsub^{H}Kim), ~6.9° C (Tsub^{H}Kaiser) and ~6.7° C (Tsub^{L}Kim).

255 Thus, our combined sample set north of the SAF fits the Tsub^{H}Kim calibration best, while the samples south of the SAF do not match the commonly used calibrations, including the two calibrations based on TEX$^L_{86}$ for (sub)polar regions (Kim et al., 2012b; Kim et al., 2010).

4.4 Influence of habitat depth on *Thaumarchaeota*-derived temperatures

Habitat depth preferences for *Thaumarchaeota* and their response to seasonality (e.g., Schouten et al., 2013) may influence
260 the TEX^H_{86}-derived temperature signals. Since *Thaumarchaeota* are distributed throughout the entire water column, the
decision to choose an optimal calibration is closely linked to an initial assumption about the water depth from which the signal
originates (Karner et al., 2001). Hence, we applied the ratio of GDGT-2 to GDGT-3 (GDGT [2]/[3]) to locate the water depth
of the temperature signal, since subsurface dwelling *Thaumarchaeota* preferentially yield GDGT-2 over the GDGT-3 (Kim et
al., 2015; Taylor et al., 2013).

265   In the global ocean the distribution of *Thaumarchaeota* appears to vary within the water column and shows an increasing
GDGT [2]/[3]-ratio with increasing depth (Dong et al., 2019; Hernández-Sánchez et al., 2014; Kim et al., 2015; Kim et al.,
2016; Schouten et al., 2012; Taylor et al., 2013). Water column samples in the Arabian Sea and along the Portuguese margin
show a GDGT [2]/[3]-ratio between <3.3 in the upper 50 m and 4.0 – 21.5 at >200 m water depth (Dong et al., 2019; Kim et
al., 2016; Schouten et al., 2012). In the South China Sea, the GDGT [2]/[3]-ratio yields <3.5 at <100 m water depth and
270 5.9 – 8.6 at water depth >300 m (Dong et al., 2019). In the Southeast Atlantic, the GDGT [2]/[3]-ratio of between 0 – 50 m
water depth is 1.9 – 3.4, 4.1 – 12.8 between 50 – 200 m water depth and 13 – 50 in water depth >200 m (Hernández-Sánchez
et al., 2014). Thus, increasing GDGT [2]/[3]-ratios may not be strictly coupled to water depths across the world ocean. The
GDGT [2]/[3]-ratio in the surface area seems similar in all regions with ~3.5, but subsurface values differ considerably. In the
Southern Atlantic, the GDGT [2]/[3]-ratio increases to up to 12.8 within 50 – 200 m water depth, whereas at the Portuguese
275 margin, the Arabian and the South China Sea, the GDGT [2]/[3]-ratio increases up to ~5.0, with oxygen content or nutrients
being the most likely reason for such non-linearities (e.g., Basse et al., 2014; Villanueva et al., 2015).

        The GDGT [2]/[3]–ratios in our extended study area vary between ~3 – 25. Values <5 (n = 7), indicating a surface signal,
are found only occasionally off New Zealand and along the Chilean Margin. The majority of samples would correspond to a
subsurface signal with a GDGT [2]/[3]–ratio >5, confirming our calibration choice ($Tsub^HKim$) for the South Pacific. Studies
280 from the Humboldt Current system, the Antarctic Peninsula and the North Pacific Gyre confirm this assumption and indicate
a subsurface rather than a surface signal (Kalanetra et al., 2009; Karner et al., 2001; Massana et al., 1998; Quiñones et al.,
2009). In the following, we will distinguish between shallower subsurface (0 – 200 m water depth) and deep subsurface
(>200 m water depth), to quantify the influence of deep subsurface-dwelling *Thaumarchaeota* to the GDGT distribution in the
sediment. In general, it is assumed that a deep subsurface water influence is comparatively small, since *Thaumarchaeota* can
285 be most effectively grazed, packed into fecal pellets, and transported to the seafloor within the photic zone (Wuchter et al.,
2005). Nevertheless, variations in the GDGT [2]/[3]-ratio across the entire study area can provide information about regions
that may be subject to a greater influence of deep subsurface dwelling *Thaumarchaeota*. Our South Pacific locations yield
differences in GDGT [2]/[3]-ratio according to three principally differing boundary or forcing conditions: A hemipelagic
continental margin setting, a deep thermocline oligotrophic gyre setting, and a SO frontal setting (**Figure 10**).

290   In the SE Pacific along the Chilean Margin, the GDGT [2]/[3]-ratio increases with increasing latitudes. Samples along the Chilean Margin (Kaiser et al., 2015) yield a mean ratio of ~6.2 to ~6.9, which implies a shallow subsurface (≥50 m water depth) habitat, with a potential increase in the amount of deeper-dwelling *Thaumarchaeota* from north to south, in line with previous studies (Quiñones et al., 2009). On the other hand, the Northern – Central Chilean Margin data show a positive correlation with both SSTs and Tsub, and the surface calibration has a comparable slope with suspended particulate matter

295   close to the surface (Kaiser et al., 2015). We assume that along the Chilean Margin and SCM, the TEX^H_{86} and TEX^L_{86} signal reflects a transition between surface and shallow subsurface habitats, where shallow subsurface habitats increasingly prevail towards higher latitudes. Additionally, the amount of deep subsurface-dwelling *Thaumarchaeota* increase with increasing distance from land e.g., site PS97/114 on the SCM is located further offshore and yields a GDGT [2]/[3]-ratio of 10.6 (3863 m water depth) compared to the mean of ~6.9 at ~1700 m water depth closer to the margin. Our assumption is supported by our

300   own results from the SW Pacific close to New Zealand, which are a good example for increasing sedimentary GDGT [2]/[3]-ratios with increasing water depths (**Figure 10**), in line with a study by Taylor et al. (2013). The SW Pacific samples close to the margin show a GDGT [2]/[3]-ratio of ~3.1 (~600 m water depth), indicating surface temperature signals. With greater distance from the margin, the GDGT [2]/[3]-ratio increases to ~9.8 (>3000 m water depth) or ~12.9 (>4000 m water depth), and thus the influence of deep subsurface-dwelling *Thaumarchaeota*.

305   Samples from the pelagic South Pacific Gyre region yield highest GDGT [2]/[3]-ratios averaging ~11.5, indicating a potentially larger contribution of deep subsurface-dwelling *Thaumarchaeota* communities in the sediment. On the other hand, no significant temperature deviations can be detected for this region (**Figure 9**). This suggests either that the influence of the deep subsurface-dwelling *Thaumarchaeota* on the temperature signal is smaller than previously thought, or that the distribution of the GDGT [2]/[3]-ratio in the subsurface in this region differs from that in the central South Pacific or continental margins.

310   In the Drake Passage, the GDGT [2]/[3]-ratios show average values of ~8.7 and are mostly higher than on the Chilean Margin, implying a more prominent influence of deep subsurface-dwelling *Thaumarchaeota* (**Figure 10**). We found GDGT [2]/[3] maxima close to the PF (~10.1), probably caused by stronger mixing, which would result in a higher abundance of deep subsurface-dwelling *Thaumarchaeota* below the northward-flowing Antarctic Surface Water layer. Values around the SACCF are ~6.7, comparable to those on the SCM, and therefore likely represent shallow subsurface habitats, with only minor

315   influence from deep subsurface-dwelling *Thaumarchaeota*. This is in line with evidence from the Antarctic Peninsula region, which shows highest abundances of *Thaumarchaeota* between ca. 40 – 100 m water depth in Antarctic Winter Water and a near-absence in the surface layer (Kalanetra et al., 2009). Samples from the Southwest Pacific (Ho et al., 2014; Jaeschke et al., 2017) show comparable results, with slightly lower mean GDGT [2]/[3]-ratios of ~8 and absolute minima of ~6.4 south of the SACCF (**Figure 10**).

320   In summary, our results suggest that GDGTs record shallower subsurface temperatures rather than surface temperatures in the study area. Samples along continental slopes tend to be less influenced by deep subsurface-dwelling *Thaumarchaeota*, while samples from the pelagic regions show a greater influence by deep subsurface-dwelling *Thaumarchaeota*. The highest influence of deep-dwelling *Thaumarchaeota* occurs in the South Pacific Gyre.

4.4 Towards an alternative southern hemisphere (sub)-polar calibration for GDGT-based temperatures

325   GDGTs south of the SAF appear to have a lower sensitivity to temperature (Kim et al., 2010), so a lower slope of the calibration line might better represent relative temperature changes (**Figure 9**). We suspect that the SAF acts as a natural boundary, leading to differential responses within the *Thaumarchaeota* communities and their respective GDGTs to changing environmental parameters. The reason for this pattern could be the increased occurrence of OH-GDGTs in polar regions. OH-GDGTs are present in lower amounts in the sediment than the isoGDGTs used in TEX^H_{86} and TEX^L_{86}, but are most abundant

330   in higher latitudes (Fietz et al., 2013; Huguet et al., 2013; Liu et al., 2020). This increased occurrence of OH-GDGTs could indicate an adaptation to cold temperatures to maintain membrane fluidity. This could simultaneously affect the relationship of TEX-based indices to temperature, requiring a separate calibration for high latitudes. OH-GDGTs also show a stronger correlation with water temperature than isoGDGTs in both the Arctic (Fietz et al., 2013) and close to Antarctica (Liu et al., 2020), so another OH-GDGT-based index (RI-OH') has been proposed for polar regions (Lü et al., 2015). Moreover, OH-

335   GDGTs were often not measured in legacy samples reported in early studies. Therefore, we here take an initial step and propose a modified TEX-based cold temperature calibration for the southern hemisphere (sub)polar region. This suggested calibration includes samples south of the SAF in the SO, and is extended by the data sets of Kim et al. (2010) and Lamping et al. (2021) with a total of n = 137 samples.

       Changes in TEX^H_{86} or general TEX_{86} indices below 5° C water temperature (according to SSTs south of the SAF in the

340   Southern Ocean) are less pronounced than above 5° C, because of a weaker correlation of the isomer Cren' to water temperatures. Thus, it is excluded in the TEX^L_{86} – index as proposed by earlier studies (Kim et al., 2010). This is in line with our results, where all TEX^L_{86} calibrations show a stronger correlation than those based on TEX^H_{86} (*cf.* determination coefficient R^2 **Figure 11**). The maximum R^2 value of 0.7 (TEX^L_{86}, subsurface) is only slightly lower than previously published values (>0.8, *cf.* **Table A1**), which is to be somewhat expected, because the scatter of both TEX^H_{86} and TEX^L_{86} indices below 5° C

345   seems to be generally larger (Ho et al., 2014).

       Based on our results, we propose a new TEX^L_{86} – based annual mean, subsurface (0 – 200 m) and surface (0 – 50 m) calibration for the Southern Ocean's polar and subpolar regions:

       $$Tsub = 14.38 * TEX^L_{86} + 8.93, \tag{1}$$

350    $$Tsub = 14.38 * TEX^L_{86} + 8.93, \tag{2}$$

       The standard error of ±0.6° C (±0.5° C) for our subsurface (surface) calibration is lower than the standard error from the previous subsurface (surface) calibration $Tsub^L$Kim (SST^LKim) with ±2.8° C (±4° C), which is probably due to the latter's lower data density. With this new calibration, just 44 (40) of the 137 samples lie outside this error range. Another major

355   difference between our calibration and $Tsub^L$Kim (SST^LKim) is the slope of the regression line being much flatter here at 14.4

(10.7) than the slope of the calibration Tsub^{L}Kim (SST^{L}Kim) with 50.8 (67.5) (**Figure 9**). This leads to a generally smaller temperature increase with an increasing TEX$^L_{86}$ index. An increase of TEX$^L_{86}$ from -0.6 to -0.5 e.g., corresponds to a temperature change of 1.4° C in our subsurface calibration and of 5.1° C in Tsub^{L}Kim.

360   Using our new calibration, we compare recalculated results with the previously used subsurface TEX$^L_{86}$ calibration Tsub^{L}Kim (**Figure 12**) on core MD03-2601 (66°03.07' S, 138°33.43' E; Kim et al., 2012b) from the eastern Indian sector of the SO covering the Holocene, where the authors acknowledged that a temperature offset existed, but within the specified calibration error range of ±2.8° C.

Temperatures based on our subsurface calibration are on average ~2.5° C colder than the ones based on the previously used subsurface calibration Tsub^{L}Kim. With our new calibration, temperatures remain relatively constant at -0.8° C, and at 1.5° C
365   with the subsurface calibration Tsub^{L}Kim between 4.8 – 3.1 ka BP. Modern temperatures near the core site agree well with core top results from our new calibration with -0.7° C (65.5° S, 138.5° E; Locarnini et al., 2006) vs. -0.8° C (our reconstruction) for the subsurface layer. The recalculated temperature increases, associated with warmer nutrient-rich modified Circumpolar Deep-Water intrusions, show an attenuated amplitude with the new calibration (**Figure 12**). The amplitude based on our new calibration is 1.2° C around 1.7 ka BP, whereas it is 4.2° C with the original subsurface calibration Tsub^{L}Kim.

370   **5 Conclusion**

In this study, we provide a new surface sediment dataset of alkenone- and GDGT-derived temperatures from the Southern Chilean Margin and the Drake Passage. In combination with previously published results from the Southern Ocean, we expanded our study area and examined which underlying calibration solution to determine upper ocean temperatures works best. In addition, we studied the possible influence of seasonal effects and the habitat water depth on the derived temperature
375   reconstructions.

For alkenone-derived SSTs, our results provide a best fit with the global core-top calibration of Müller et al. (1998). On a regional scale, the Southern Chilean Margin and the Drake Passage show a small seasonal effect of ~1° C towards warmer SSTs south of ~50° S, albeit well within the ±1.5° C standard error for alkenone derived SSTs (Müller et al., 1998). Excluding local influences, the seasonal effect in the DP is slightly higher at about ~2° C and no longer within the error range of calibration
380   by Müller et al. (1998). In contrast, the samples from the Central Southern Pacific Ocean show no clear seasonal trend. Causes for this difference between the two areas may be increased seasonal provision of nutrients or more pronounced stratification at the sites proximal to continental runoff along the Chilean margin during late summer time.

GDGT-based temperatures show a more complex pattern, which necessitates choosing the temperature calibration carefully, depending on the area. The optimal calibration for GDGT-based temperature reconstructions in the South Pacific is
385   the subsurface calibration Tsub (Kim et al., 2012a), for samples north of the Sub-Antarctic Front, in line with evidence from compiled GDGT [2]/[3]-ratios, which indicate a subsurface of 0 to 200 m water depth, rather than surface habitat depth

throughout the study area. South of the Sub-Antarctic Front, all existing calibrations overestimate local WOA05-derived temperatures.

As a result, we recommend to establish two new Southern Ocean calibrations for GDGT-based temperature reconstructions
390 and attempt to improve temperature calculations for the Pacific sector of the Southern Ocean, based on the TEX^L_{86} index. Our new calibration for subpolar and polar areas yields lower absolute subsurface temperatures, as well as lower relative changes within the commonly accepted standard error range when compared to instrumental reference data. Since our study was restricted to a mostly regional dataset, we recommend to extend both the geographical area coverage in subpolar and polar regions and the sample density for future works. Furthermore, the influence of seasonality and habitat on signal incorporation
395 should be investigated to assess how strongly these factors affect paleo-temperature reconstructions based on GDGTs.

Appendix A

Table A1: Common indices and their most important temperature calibrations for alkenones and GDGTs, with their determination coefficients and abbreviations used in this paper.

	Equation	R^2	Abbreviation	References
1	$U^{K'}_{37} = [C_{37:2}] / [C_{37:2}] + [C_{37:3}]$			Prahl and Wakeham (1987)
2	$SST = (U^{K'}_{37} - 0.043) / 0.033$	0.994		Prahl and Wakeham (1987)
3	$SST = (U^{K'}_{37} - 0.039) / 0.034$	0.994	Prahl88	Prahl et al. (1988)
4	$SST = (U^{K'}_{37} - 0.044) / 0.033$	0.958	Müller98	Müller et al. (1998)
5	$SST = (U^{K'}_{37} + 0.082) / 0.038$	0.921	Sikes97	Sikes et al. (1997)
6	$TEX_{86} = \dfrac{[2] + [3] + [Cren']}{[1] + [2] + [3] + [Cren']}$			Schouten et al. (2002)
7	$TEX^H_{86} = log\dfrac{[2] + [3] + [Cren']}{[1] + [2] + [3] + [Cren']}$			Kim et al. (2010)
8	$TEX^L_{86} = log\dfrac{[2]}{[1] + [2] + [3]}$			Kim et al. (2010)
9	$SST = 68.4 * TEX^H_{86} + 38.6$	0.87	$SST^H Kim$	Kim et al. (2010)

10	$Tsub = 54.7 * TEX^H_{86} + 30.7$	0.84	$Tsub^HKim$	Kim et al. (2012a)
11	$SST = 59.6 * TEX^H_{86} + 33$	0.91	$SST^HKaiser$	Kaiser et al. (2015)
12	$Tsub = 32.1 * TEX^H_{86} + 21.5$	0.86	$Tsub^HKaiser$	Kaiser et al. (2015)
13	$SST = 67.5 * TEX^L_{86} + 46.9$	0.86	SST^LKim	Kim et al. (2010)
14	$Tsub = 50.8 * TEX^L_{86} + 36.1$	0.87	$Tsub^LKim$	Kim et al. (2012b)

400   **Table A2: Surface sediment sample results of this study.**

	Station	Latitude	Longitude	Depth [m]	$U^{K'}_{37}$	TEX^H_{86}	TEX^L_{86}
			Southern Chilean Margin				
1	PS97/139-1	52° 26.56' S	75° 42.42' W	640	0.40	-0.40	-0.58
2	PS97/134-1	52° 40.97' S	75° 34.85' W	1075.1	0.36	-0.39	-0.54
3	PS97/132-2	52° 37.01' S	75° 35.14' W	843	0.38	-0.47	-0.60
4	PS97/131-1	52° 39.58' S	75° 33.97' W	1028.2	0.35	-0.39	-0.53
5	PS97/129-2	53° 19.28' S	75° 12.84' W	1879.4	0.34	-0.41	-0.54
6	PS97/128-1	53° 38.04' S	75° 32.71' W	2293.7	0.32	-0.42	-0.54
7	PS97/122-2	54° 5.85' S	74° 54.89' W	2560	0.31	-0.41	-0.53
8	PS97/114-1	54° 34.68' S	76° 38.85' W	3863	0.26	-0.41	-0.50
9	PS97/027-1	54° 23.05' S	74° 36.30' W	2349.2	0.28	-0.41	-0.53
10	PS97/024-2	54° 35.27' S	73° 57.30' W	1272.8	-	-	-
11	PS97/022-1	54° 42.03' S	73° 48.38' W	1615.1	0.27	-0.41	-0.55
12	PS97/021-1	55° 6.91' S	72° 40.09' W	1840.4	0.30	-0.41	-0.54
13	PS97/020-1	55° 30.80' S	71° 38.22' W	2104.3	0.27	-0.42	-0.54
14	PS97/015-2	55° 43.89' S	70° 53.55' W	1886.3	0.31	-0.42	-0.55
15	PS97/094-1	57° 0.17' S	70° 58.32' W	3993.4	0.31	-0.39	-0.52
16	PS97/093-3	57° 29.92' S	70° 16.57' W	3782.2	0.36	-0.42	-0.54
17	PS97/097-1	57° 3.27' S	67° 4.00' W	2318.6	0.30	-0.42	-0.53
18	PS97/096-1	56° 4.53' S	66° 8.96' W	1620.7	0.31	-0.44	-0.55
19	PS97/095-1	56° 14.68' S	66° 14.95' W	1652.1	0.25	-0.43	-0.55
			Drake Passage Shackleton Fracture Zone				
20	PS97/089-2	58° 13.60' S	62° 43.63' W	3431.9	0.18	-0.43	-0.56
21	PS97/086-2	58° 38.65' S	61° 23.82' W	2968.9	0.15	-0.45	-0.56
22	PS97/085-2	58° 21.28' S	62° 10.07' W	3090.7	0.16	-0.43	-0.55

23*	PS97/084-2	58° 52.14' S	60° 51.91' W	3617.4	0.10	-0.46	-0.58
24*	PS97/083-1	58° 59.65' S	60° 34.28' W	3756.3	0.12	-0.49	-0.60
25*	PS97/080-2	59° 40.49' S	59° 37.86' W	3112.7	0.12	-0.46	-0.56
26*	PS97/079-1	60° 8.55' S	58° 59.42' W	3539.3	0.07	-0.48	-0.61
Drake Passage Phoenix Antarctic Ridge							
27*	PS97/042-1	59° 50.62' S	66° 5.77' W	4172	0.12	-0.43	-0.54
28*	PS97/044-1	60° 36.80' S	66° 1.34' W	1202.8	-	-0.48	-0.57
29*	PS97/045-1	60° 34.27' S	66° 5.67' W	2292	0.14	-0.47	-0.55
30*	PS97/046-6	60° 59.74' S	65° 21.40' W	2802.7	0.13	-0.45	-0.56
31*	PS97/048-1	61° 26.40' S	64° 53.27' W	3455.2	0.14	-0.42	-0.55
32*	PS97/049-2	61° 40.28' S	64° 57.74' W	3752.2	0.14	-0.47	-0.58
33*	PS97/052-3	62° 29.93' S	64° 17.63' W	2889.8	-	-0.46	-0.60

* GDGTs Lamping et al. (2021); Alkenone *this study*

Data availability. All locations and the three main indices of the new 33 samples of this study are available in **Table A2**.

405 **Author contributions.** The study was conceived by JRH and LL-J; MEV, JRH, JH and NR contributed with analytical tools; JRH, LL-J, JK, AJ analyzed data; JRH drafted the paper and figures; LL-J supervised the study. All authors contributed to the interpretation and discussion of the results as well as commented on, or contributed to the draft and final version of the manuscript.

410 **Acknowledgements.** We thank master and crew of R/V Polarstern, as well as the science party for their professional support on expedition PS97 "Paleo-Drake". We thank Sophie Ehrhardt for providing unpublished alkenone data. We thank the technicians Walter Luttmer and Denise Diekstall for their support in the laboratory. We acknowledge funding through the AWI institutional research programs "PACES-II" and "Changing Earth – Sustaining our Future", as well as through the REKLIM initiative.

415

Financial support. This research has been supported by the AWI institutional research programs "PACE-II" and "Changing Earth – Sustaining our Future", as well as through the REKLIM initiative.

Competing Interests. The authors declare no conflict of interest.

420

References

Basse, A., Zhu, C., Versteegh, G. J. M., Fischer, G., Hinrichs, K. U., and Mollenhauer, G.: Distribution of intact and core tetraether lipids in water column profiles of suspended particulate matter off Cape Blanc, NW Africa, Organic Geochemistry, 72, 1-13, 10.1016/j.orggeochem.2014.04.007, 2014.

425 Baumann, K.-H., Andruleit, H., Böckel, B., Geisen, M., and Kinkel, H.: The significance of extant coccolithophores as indicators of ocean water masses, surface water temperature, and palaeoproductivity: a review, Paläontologische Zeitschrift, 79, 93-112, 10.1007/bf03021756, 2005.

Brochier-Armanet, C., Boussau, B., Gribaldo, S., and Forterre, P.: Mesophilic Crenarchaeota: proposal for a third archaeal phylum, the Thaumarchaeota, Nat Rev Microbiol, 6, 245-252, 10.1038/nrmicro1852, 2008.

430 Caniupán, M., Lamy, F., Lange, C. B., Kaiser, J., Kilian, R., Arz, H. W., León, T., Mollenhauer, G., Sandoval, S., De Pol-Holz, R., Pantoja, S., Wellner, J., and Tiedemann, R.: Holocene sea-surface temperature variability in the Chilean fjord region, Quaternary Research, 82, 342-353, 10.1016/j.yqres.2014.07.009, 2014.

D'Hondt, S., Spivack, A. J., Pockalny, R., Ferdelman, T. G., Fischer, J. P., Kallmeyer, J., Abrams, L. J., Smith, D. C., Graham, D., Hasiuk, F., Schrum, H., and Stancin, A. M.: Subseafloor sedimentary life in the South Pacific Gyre, Proc Natl Acad Sci U
435 S A, 106, 11651-11656, 10.1073/pnas.0811793106, 2009.

Dávila, P. M., Figueroa, D., and Müller, E.: Freshwater input into the coastal ocean and its relation with the salinity distribution off austral Chile (35–55°S), Continental Shelf Research, 22, 521-534, 10.1016/s0278-4343(01)00072-3, 2002.

Dong, L., Li, Z. Y., and Jia, G. D.: Archaeal ammonia oxidation plays a part in late Quaternary nitrogen cycling in the South China Sea, Earth and Planetary Science Letters, 509, 38-46, 10.1016/j.epsl.2018.12.023, 2019.

440 Epstein, B. L., D'Hondt, S., and Hargraves, P. E.: The possible metabolic role of C37 alkenones in Emiliania huxleyi, Organic Geochemistry, 32, 867-875, 10.1016/s0146-6380(01)00026-2, 2001.

Fietz, S., Huguet, C., Rueda, G., Hambach, B., and Rosell-Mele, A.: Hydroxylated isoprenoidal GDGTs in the Nordic Seas, Marine Chemistry, 152, 1-10, 10.1016/j.marchem.2013.02.007, 2013.

Garreaud, R., Lopez, P., Minvielle, M., and Rojas, M.: Large-Scale Control on the Patagonian Climate, Journal of Climate,
445 26, 215-230, 10.1175/Jcli-D-12-00001.1, 2013.

Herbert, T. D.: Review of alkenone calibrations (culture, water column, and sediments), Geochemistry Geophysics Geosystems, 2, 10.1029/2000gc000055, 2001.

Herbert, T. D., Peterson, L. C., Lawrence, K. T., and Liu, Z.: Tropical ocean temperatures over the past 3.5 million years, Science, 328, 1530-1534, 10.1126/science.1185435, 2010.

450   Hernández-Sánchez, M. T., Woodward, E. M. S., Taylor, K. W. R., Henderson, G. M., and Pancost, R. D.: Variations in GDGT distributions through the water column in the South East Atlantic Ocean, Geochimica et Cosmochimica Acta, 132, 337-348, 10.1016/j.gca.2014.02.009, 2014.

Ho, S. L., Mollenhauer, G., Fietz, S., Martinez-Garcia, A., Lamy, F., Rueda, G., Schipper, K., Meheust, M., Rosell-Mele, A., Stein, R., and Tiedemann, R.: Appraisal of TEX86 and TEX86L thermometries in subpolar and polar regions, Geochimica Et
455   Cosmochimica Acta, 131, 213-226, 10.1016/j.gca.2014.01.001, 2014.

Hopmans, E. C., Schouten, S., and Damste, J. S. S.: The effect of improved chromatography on GDGT-based palaeoproxies, Organic Geochemistry, 93, 1-6, 10.1016/j.orggeochem.2015.12.006, 2016.

Huguet, C., Fietz, S., and Rosell-Mele, A.: Global distribution patterns of hydroxy glycerol dialkyl glycerol tetraethers, Organic Geochemistry, 57, 107-118, 10.1016/j.orggeochem.2013.01.010, 2013.

460   Jaeschke, A., Wengler, M., Hefter, J., Ronge, T. A., Geibert, W., Mollenhauer, G., Gersonde, R., and Lamy, F.: A biomarker perspective on dust, productivity, and sea surface temperature in the Pacific sector of the Southern Ocean, Geochimica Et Cosmochimica Acta, 204, 120-139, 10.1016/j.gca.2017.01.045, 2017.

Kaiser, J., Schouten, S., Kilian, R., Arz, H. W., Lamy, F., and Damste, J. S. S.: Isoprenoid and branched GDGT-based proxies for surface sediments from marine, fjord and lake environments in Chile, Organic Geochemistry, 89-90, 117-127,
465   10.1016/j.orggeochem.2015.10.007, 2015.

Kalanetra, K. M., Bano, N., and Hollibaugh, J. T.: Ammonia-oxidizing Archaea in the Arctic Ocean and Antarctic coastal waters, Environ Microbiol, 11, 2434-2445, 10.1111/j.1462-2920.2009.01974.x, 2009.

Karner, M. B., DeLong, E. F., and Karl, D. M.: Archaeal dominance in the mesopelagic zone of the Pacific Ocean, Nature, 409, 507-510, 10.1038/35054051, 2001.

470   Kim, J. H., Villanueva, L., Zell, C., and Damste, J. S. S.: Biological source and provenance of deep-water derived isoprenoid tetraether lipids along the Portuguese continental margin, Geochimica Et Cosmochimica Acta, 172, 177-204, 10.1016/j.gca.2015.09.010, 2016.

Kim, J. H., Romero, O. E., Lohmann, G., Donner, B., Laepple, T., Haam, E., and Damste, J. S. S.: Pronounced subsurface cooling of North Atlantic waters off Northwest Africa during Dansgaard-Oeschger interstadials, Earth and Planetary Science
475   Letters, 339, 95-102, 10.1016/j.epsl.2012.05.018, 2012a.

Kim, J. H., Crosta, X., Willmott, V., Renssen, H., Bonnin, J., Helmke, P., Schouten, S., and Damste, J. S. S.: Holocene subsurface temperature variability in the eastern Antarctic continental margin, Geophysical Research Letters, 39, 10.1029/2012gl051157, 2012b.

Kim, J. H., van der Meer, J., Schouten, S., Helmke, P., Willmott, V., Sangiorgi, F., Koc, N., Hopmans, E. C., and Damste, J.
480   S. S.: New indices and calibrations derived from the distribution of crenarchaeal isoprenoid tetraether lipids: Implications for
       past sea surface temperature reconstructions, Geochimica Et Cosmochimica Acta, 74, 4639-4654, 10.1016/j.gca.2010.05.027,
       2010.

Kim, J. H., Schouten, S., Rodrigo-Gamiz, M., Rampen, S., Marino, G., Huguet, C., Helmke, P., Buscail, R., Hopmans, E. C.,
       Pross, J., Sangiorgi, F., Middelburg, J. B. M., and Damste, J. S. S.: Influence of deep-water derived isoprenoid tetraether lipids
485   on the TEX86H paleothermometer in the Mediterranean Sea, Geochimica Et Cosmochimica Acta, 150, 125-141,
       10.1016/j.gca.2014.11.017, 2015.

Koenig, Z., Provost, C., Ferrari, R., Sennechael, N., and Rio, M. H.: Volume transport of the Antarctic Circumpolar Current:
       Production and validation of a 20 year long time series obtained from in situ and satellite observations, Journal of Geophysical
       Research-Oceans, 119, 5407-5433, 10.1002/2014jc009966, 2014.

490   Lamping, N., Muller, J., Hefter, J., Mollenhauer, G., Haas, C., Shi, X. X., Vorrath, M. E., Lohmann, G., and Hillenbrand, C.
       D.: Evaluation of lipid biomarkers as proxies for sea ice and ocean temperatures along the Antarctic continental margin,
       Climate of the Past, 17, 2305-2326, 10.5194/cp-17-2305-2021, 2021.

Lamy, F.: The Expedition PS97 of the Research Vessel POLARSTERN to the Drake Passage in 2016 , Berichte zur Polar-
       und Meeresforschung = Reports on polar and marine research, Bremerhaven, Alfred Wegener Institute for Polar and Marine
495   Research, 571 p., 10.2312/BzPM_0701_2016, 2016.

Lamy, F., Kilian, R., Arz, H. W., Francois, J. P., Kaiser, J., Prange, M., and Steinke, T.: Holocene changes in the position and
       intensity of the southern westerly wind belt, Nature Geoscience, 3, 695-699, 10.1038/Ngeo959, 2010.

Lamy, F., Gersonde, R., Winckler, G., Esper, O., Jaeschke, A., Kuhn, G., Ullermann, J., Martinez-Garcia, A., Lambert, F., and
       Kilian, R.: Increased dust deposition in the Pacific Southern Ocean during glacial periods, Science, 343, 403-407,
500   10.1126/science.1245424, 2014.

Liu, R. J., Han, Z. B., Zhao, J., Zhang, H. F., Li, D., Ren, J. Y., Pan, J. M., and Zhang, H. S.: Distribution and source of glycerol
       dialkyl glycerol tetraethers (GDGTs) and the applicability of GDGT-based temperature proxies in surface sediments of Prydz
       Bay, East Antarctica, Polar Research, 39, 10.33265/polar.v39.3557, 2020.

Locarnini, R. A., Mishonov, A. V., Antonov, J. I., Boyer, T. P., and Garcia, H. E.: World Ocean Atlas 2005, Volume 1:
505   Temperature, S. Levitus, Ed. NOAA Atlas NESDIS 61 [dataset], 2006.

Locarnini, R. A., Mishonov, A. V., Antonov, J. I., Boyer, T. P., Garcia, H. E., Baranova, O. K., Zweng, M. M., and Johnson,
       D. R.: World Ocean Atlas 2009, Volume 1: Temperature S. Levitus, Ed., NOAA Atlas NESIDIS 68, U.S. Government Printing
       Office, Washington, D.C., 184 pp., 2010.

Lü, X., Liu, X.-L., Elling, F. J., Yang, H., Xie, S., Song, J., Li, X., Yuan, H., Li, N., and Hinrichs, K.-U.: Hydroxylated
510   isoprenoid GDGTs in Chinese coastal seas and their potential as a paleotemperature proxy for mid-to-low latitude marginal
       seas, Organic Geochemistry, 89-90, 31-43, 10.1016/j.orggeochem.2015.10.004, 2015.

Massana, R., Taylor, L. J., Murray, A. E., Wu, K. Y., Jeffrey, W. H., and DeLong, E. F.: Vertical distribution and temporal variation of marine planktonic archaea in the Gerlache Strait, Antarctica, during early spring, Limnology and Oceanography, 43, 607-617, 10.4319/lo.1998.43.4.0607, 1998.

515 Max, L., Lembke-Jene, L., Zou, J., Shi, X., and Tiedemann, R.: Evaluation of reconstructed sea surface temperatures based on U37k′ from sediment surface samples of the North Pacific, Quaternary Science Reviews, 243, 10.1016/j.quascirev.2020.106496, 2020.

Méheust, M., Fahl, K., and Stein, R.: Variability in modern sea surface temperature, sea ice and terrigenous input in the sub-polar North Pacific and Bering Sea: Reconstruction from biomarker data, Organic Geochemistry, 57, 54-64, 520 10.1016/j.orggeochem.2013.01.008, 2013.

Müller, P. J., Kirst, G., Ruhland, G., von Storch, I., and Rosell-Melé, A.: Calibration of the alkenone paleotemperature index U37K′ based on core-tops from the eastern South Atlantic and the global ocean (60°N-60°S), Geochimica et Cosmochimica Acta, 62, 1757-1772, 10.1016/s0016-7037(98)00097-0, 1998.

Murray, A. E., Preston, C. M., Massana, R., Taylor, L. T., Blakis, A., Wu, K., and DeLong, E. F.: Seasonal and spatial 525 variability of bacterial and archaeal assemblages in the coastal waters near Anvers Island, Antarctica, Appl Environ Microbiol, 64, 2585-2595, 10.1128/AEM.64.7.2585-2595.1998, 1998.

Orsi, A. H., Whitworth, T., and Nowlin, W. D.: On the Meridional Extent and Fronts of the Antarctic Circumpolar Current, Deep-Sea Research Part I-Oceanographic Research Papers, 42, 641-673, 10.1016/0967-0637(95)00021-W, 1995.

Popp, B. N., Kenig, F., Wakeham, S. G., Laws, E. A., and Bidigare, R. R.: Does growth rate affect ketone unsaturation and 530 intracellular carbon isotopic variability inEmiliania huxleyi?, Paleoceanography, 13, 35-41, 10.1029/97pa02594, 1998.

Prahl, F. G. and Wakeham, S. G.: Calibration of unsaturation patterns in long-chain ketone compositions for palaeotemperature assessment, Nature, 330, 367-369, 10.1038/330367a0, 1987.

Prahl, F. G., Mix, A. C., and Sparrow, M. A.: Alkenone paleothermometry: Biological lessons from marine sediment records off western South America, Geochimica Et Cosmochimica Acta, 70, 101-117, 10.1016/j.gca.2005.08.023, 2006.

535 Prahl, F. G., Muehlhausen, L. A., and Zahnle, D. L.: Further Evaluation of Long-Chain Alkenones as Indicators of Paleoceanographic Conditions, Geochimica Et Cosmochimica Acta, 52, 2303-2310, 10.1016/0016-7037(88)90132-9, 1988.

Prahl, F. G., Rontani, J. F., Zabeti, N., Walinsky, S. E., and Sparrow, M. A.: Systematic pattern in U-37(K ') - Temperature residuals for surface sediments from high latitude and other oceanographic settings, Geochimica Et Cosmochimica Acta, 74, 131-143, 10.1016/j.gca.2009.09.027, 2010.

540 Quiñones, R. A., Levipan, H. A., and Urrutia, H.: Spatial and temporal variability of planktonic archaeal abundance in the Humboldt Current System off Chile, Deep Sea Research Part II: Topical Studies in Oceanography, 56, 1073-1082, 10.1016/j.dsr2.2008.09.012, 2009.

Rintoul, S. R.: The global influence of localized dynamics in the Southern Ocean, Nature, 558, 209-218, 10.1038/s41586-018-0182-3, 2018.

545 Saavedra-Pellitero, M., Baumann, K. H., Flores, J. A., and Gersonde, R.: Biogeographic distribution of living coccolithophores in the Pacific sector of the Southern Ocean, Marine Micropaleontology, 109, 1-20, 10.1016/j.marmicro.2014.03.003, 2014.

Saavedra-Pellitero, M., Baumann, K. H., Fuertes, M. A., Schulz, H., Marcon, Y., Vollmar, N. M., Flores, J. A., and Lamy, F.: Calcification and latitudinal distribution of extant coccolithophores across the Drake Passage during late austral summer 2016, Biogeosciences, 16, 3679-3702, 10.5194/bg-16-3679-2019, 2019.

550 Schneider, C., Glaser, M., Kilian, R., Santana, A., Butorovic, N., and Casassa, G.: Weather Observations Across the Southern Andes at 53°S, Physical Geography, 24, 97-119, 10.2747/0272-3646.24.2.97, 2003.

Schouten, S., Hopmans, E. C., and Damste, J. S. S.: The organic geochemistry of glycerol dialkyl glycerol tetraether lipids: A review, Organic Geochemistry, 54, 19-61, 10.1016/j.orggeochem.2012.09.006, 2013.

Schouten, S., Hopmans, E. C., Schefuß, E., and Sinninghe Damsté, J. S.: Distributional variations in marine crenarchaeotal
555 membrane lipids: a new tool for reconstructing ancient sea water temperatures?, Earth and Planetary Science Letters, 204, 265-274, 10.1016/s0012-821x(02)00979-2, 2002.

Schouten, S., Huguet, C., Hopmans, E. C., Kienhuis, M. V., and Damste, J. S.: Analytical methodology for TEX86 paleothermometry by high-performance liquid chromatography/atmospheric pressure chemical ionization-mass spectrometry, Anal Chem, 79, 2940-2944, 10.1021/ac062339v, 2007.

560 Schouten, S., Pitcher, A., Hopmans, E. C., Villanueva, L., van Bleijswijk, J., and Damste, J. S. S.: Intact polar and core glycerol dibiphytanyl glycerol tetraether lipids in the Arabian Sea oxygen minimum zone: I. Selective preservation and degradation in the water column and consequences for the TEX86, Geochimica Et Cosmochimica Acta, 98, 228-243, 10.1016/j.gca.2012.05.002, 2012.

Sikes, E. L., Volkman, J. K., Robertson, L. G., and Pichon, J. J.: Alkenones and alkenes in surface waters and sediments of
565 the Southern Ocean: Implications for paleotemperature estimation in polar regions, Geochimica Et Cosmochimica Acta, 61, 1495-1505, 10.1016/S0016-7037(97)00017-3, 1997.

Strub, P. T., Mesías, J. M., Montecino, V., Rutllant, J., and Salinas, S.: Chapter 10. Coastal ocean circulation off western south america coastal segment, in: The Sea, edited by: Robinson, A. R., and Kenneth, H. B., 273-313, 1998.

Taylor, K. W. R., Huber, M., Hollis, C. J., Hernandez-Sanchez, M. T., and Pancost, R. D.: Re-evaluating modern and
570 Palaeogene GDGT distributions: Implications for SST reconstructions, Global and Planetary Change, 108, 158-174, 10.1016/j.gloplacha.2013.06.011, 2013.

Toyos, M. H., Winckler, G., Arz, H. W., Lembke-Jene, L., Lange, C. B., Kuhn, G., and Lamy, F.: Variations in export production, lithogenic sediment transport and iron fertilization in the Pacific sector of the Drake Passage over the past 400 kyr, Climate of the Past, 18, 147-166, 10.5194/cp-18-147-2022, 2022.

575 Villanueva, L., Schouten, S., and Sinninghe Damste, J. S.: Depth-related distribution of a key gene of the tetraether lipid biosynthetic pathway in marine Thaumarchaeota, Environ Microbiol, 17, 3527-3539, 10.1111/1462-2920.12508, 2015.

Vollmar, N. M., Baumann, K. H., Saavedra-Pellitero, M., and Hernandez-Almeida, I.: Distribution of coccoliths in surface sediments across the Drake Passage and calcification of Emiliania huxleyi morphotypes, Biogeosciences, 19, 585-612, 10.5194/bg-19-585-2022, 2022.

580 Vorrath, M. E., Muller, J., Rebolledo, L., Cardenas, P., Shi, X. X., Esper, O., Opel, T., Geibert, W., Munoz, P., Haas, C., Kuhn, G., Lange, C. B., Lohmann, G., and Mollenhauer, G.: Sea ice dynamics in the Bransfield Strait, Antarctic Peninsula, during past 240 years: a multi-proxy intercomparison study, Climate of the Past, 16, 2459-2483, 10.5194/cp-16-2459-2020, 2020.

Watson, A. J., Vallis, G. K., and Nikurashin, M.: Southern Ocean buoyancy forcing of ocean ventilation and glacial atmospheric CO2, Nature Geoscience, 8, 10.1038/Ngeo2538, 2015.

585 Wuchter, C., Schouten, S., Wakeham, S. G., and Sinninghe Damsté, J. S.: Temporal and spatial variation in tetraether membrane lipids of marine Crenarchaeota in particulate organic matter: Implications for TEX86paleothermometry, Paleoceanography, 20, 10.1029/2004pa001110, 2005.
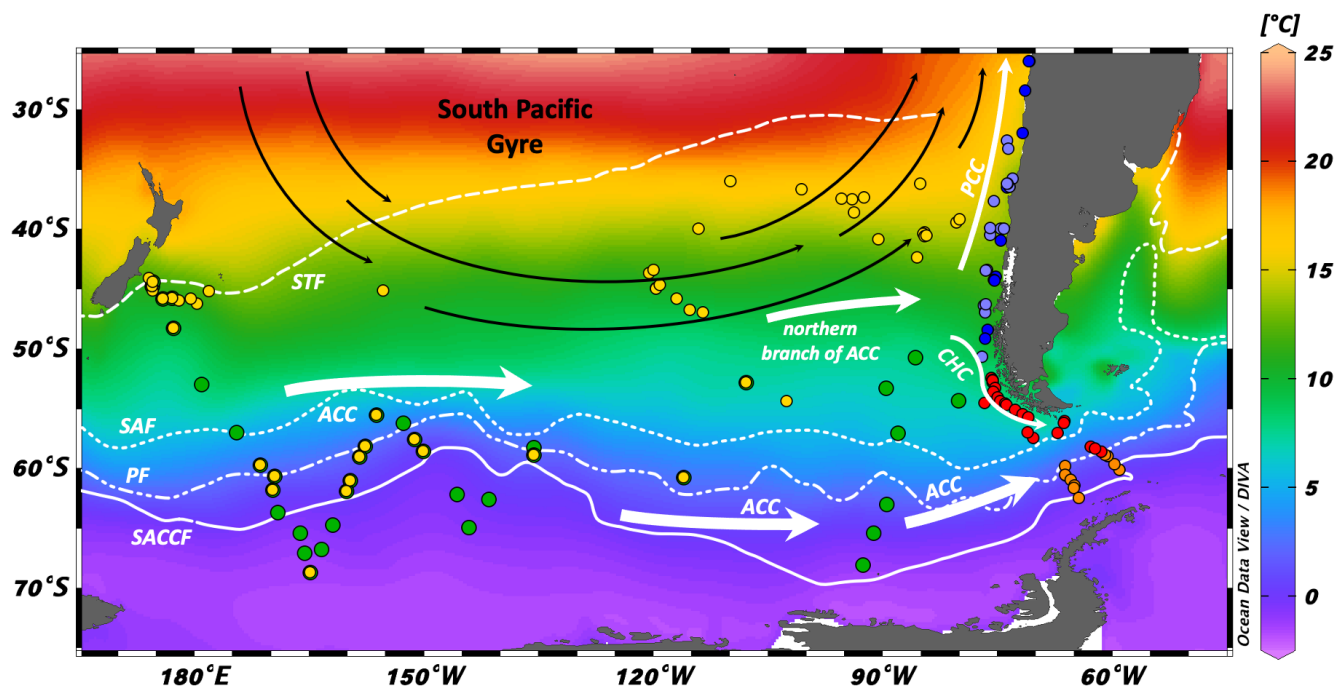
Figure 1: Map with SSTs (WOA05; Locarnini et al., 2006) of the extended study area and sample locations. ACC: Antarctic Circumpolar Current; PCC: Peru-Chile Current; CHC: Cape Horn Current; STF: Subtropical Front; SAF: Subantarctic Front; PF: Polar Front; SACCF: Southern ACC Front. Red dots: Southern Chilean Margin and Drake Passage samples (this study); Orange dots: Drake Passage samples (Lamping et al., 2021; this study); Light blue dots: Northern – Central Chilean Margin samples (Prahl et al., 2006; Prahl et al., 2010); Dark blue dots: Northern – Central Chilean Margin samples (Kaiser et al., 2015); Yellow dots: South Pacific Gyre, Central South Pacific and New Zealand Margin samples (Jaeschke et al., 2017); Green dots: Central South Pacific and New Zealand Margin samples (Ho et al., 2014).
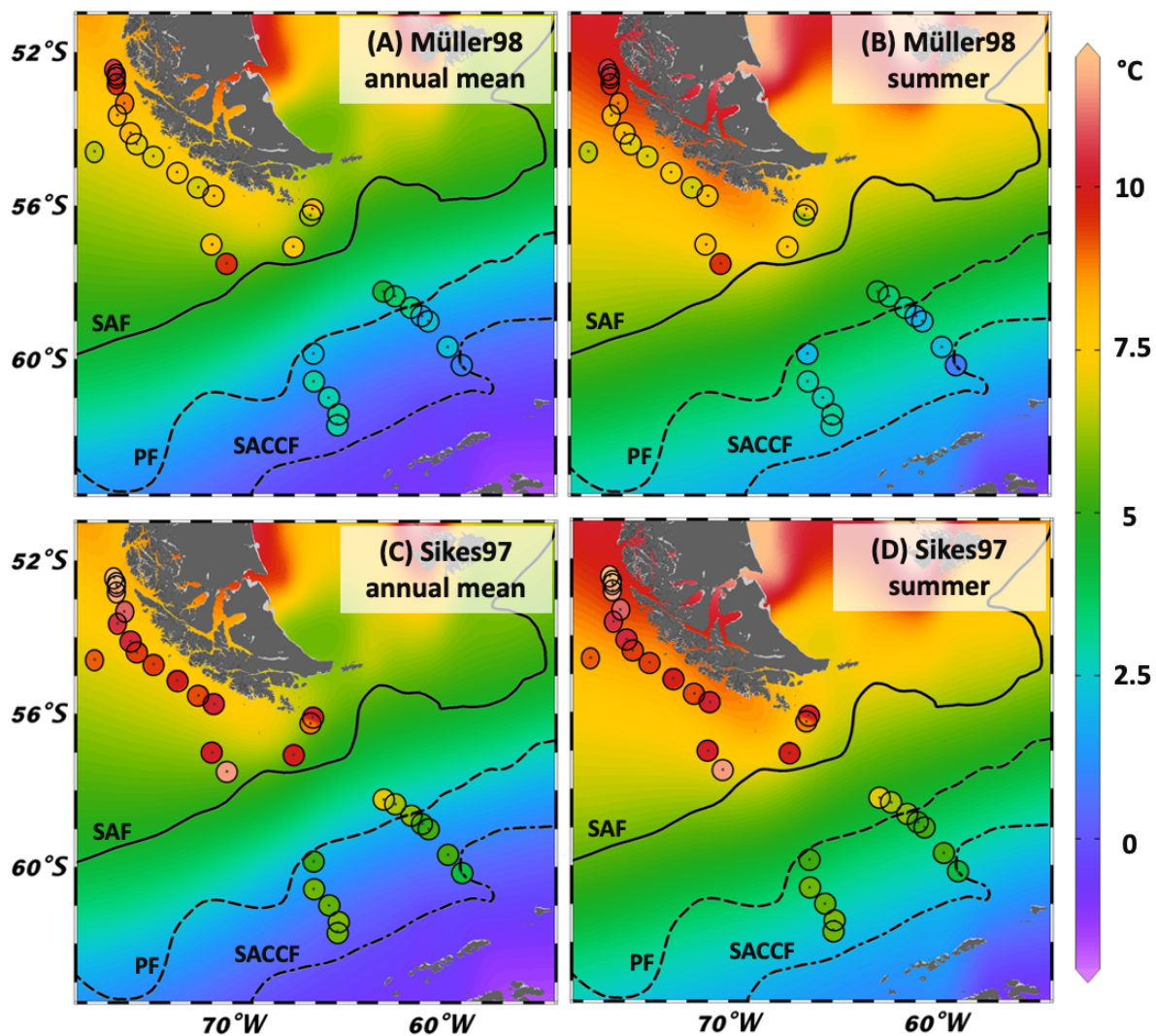
Figure 2: Map of reconstructed SST values for $U^{K'}_{37}$ (this study). Background gridded temperatures: WOA05 data (WOA05; Locarnini et al., 2006), colored dots are calculated SSTs. (A) WOA05 annual mean SSTs with Müller98 calibration; (B) WOA05 summer SSTs with Müller98 calibration; (C) WOA05 annual mean SSTs with Sikes97 calibration; (D) WOA05 summer SSTs with Sikes97 calibration.

600
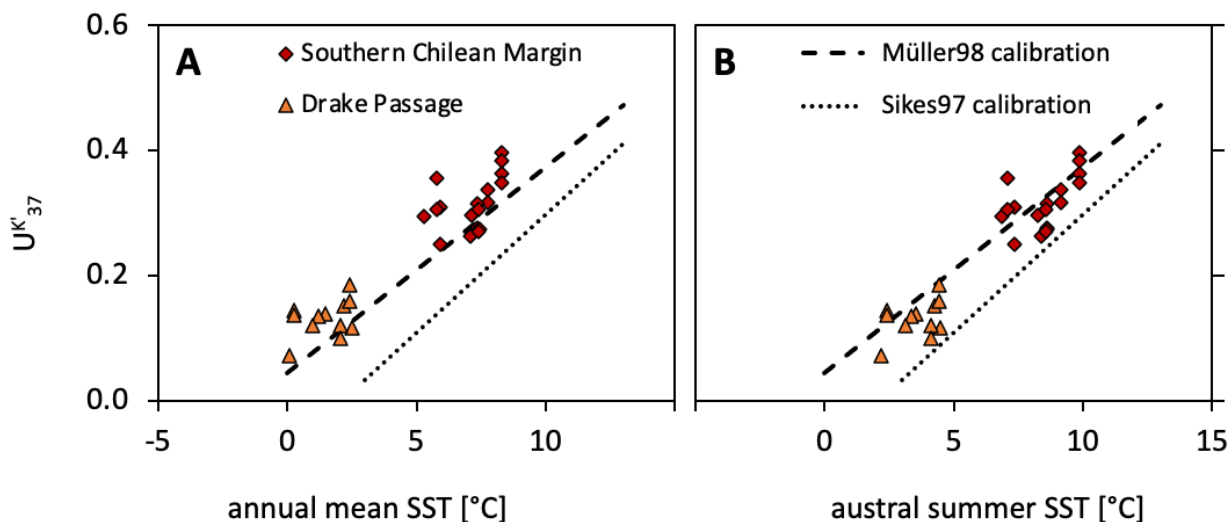
Figure 3: Comparison of $U^{K'}_{37}$ index (this study) with modern SSTs at 10 m water depth (WOA05; Locarnini et al., 2006), for (A) annual mean SSTs, and (B) austral summer SSTs, corresponding to January – March.
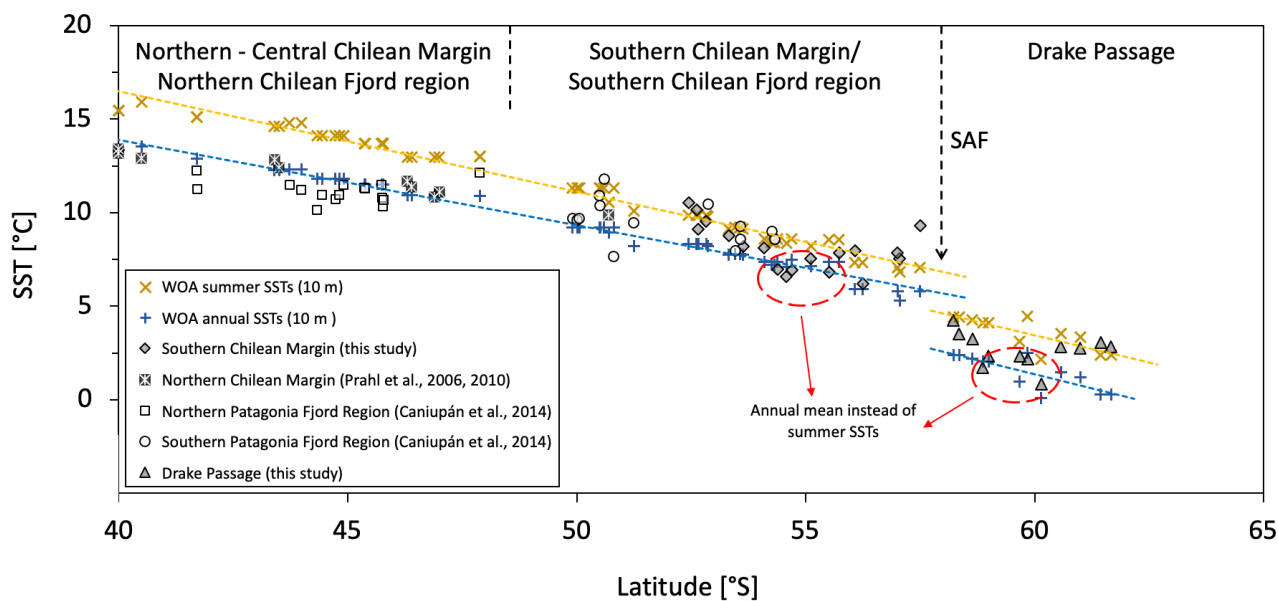
Figure 4: Comparison of ocean and fjord samples in the Chilean region. Yellow and Blue dashed lines show the meridional temperature evolution during summer and annual mean at 10 m water depth, respectively. Annual mean and summer data were taken from WOA09 (Locarnini et al., 2010) for the samples of Caniupán et al. (2014) and WOA05 (Locarnini et al., 2006) for Prahl et al. (2006, 2010) and this study.

Figure 5: (A) and (B): Compilation of $U^{K'}_{37}$ index of this study and the expanded South Pacific study area with SSTs at 10 m water depth for annual mean and austral summer, respectively (WOA05; Locarnini et al., 2006). **(C) and (D):** Residuals of the local SSTs at 10 m water depth for the annual mean and austral summer (WOA05; Locarnini et al., 2006) subtracted by the Müller98 calculated SSTs. Temperature range of dotted line shows the standard error of the temperature calibration of ±1.5° C by Müller et al. (1998). Site PS75/088-6 (Jaeschke et al., 2017) was excluded due to unrealistic high temperatures of >10° C.
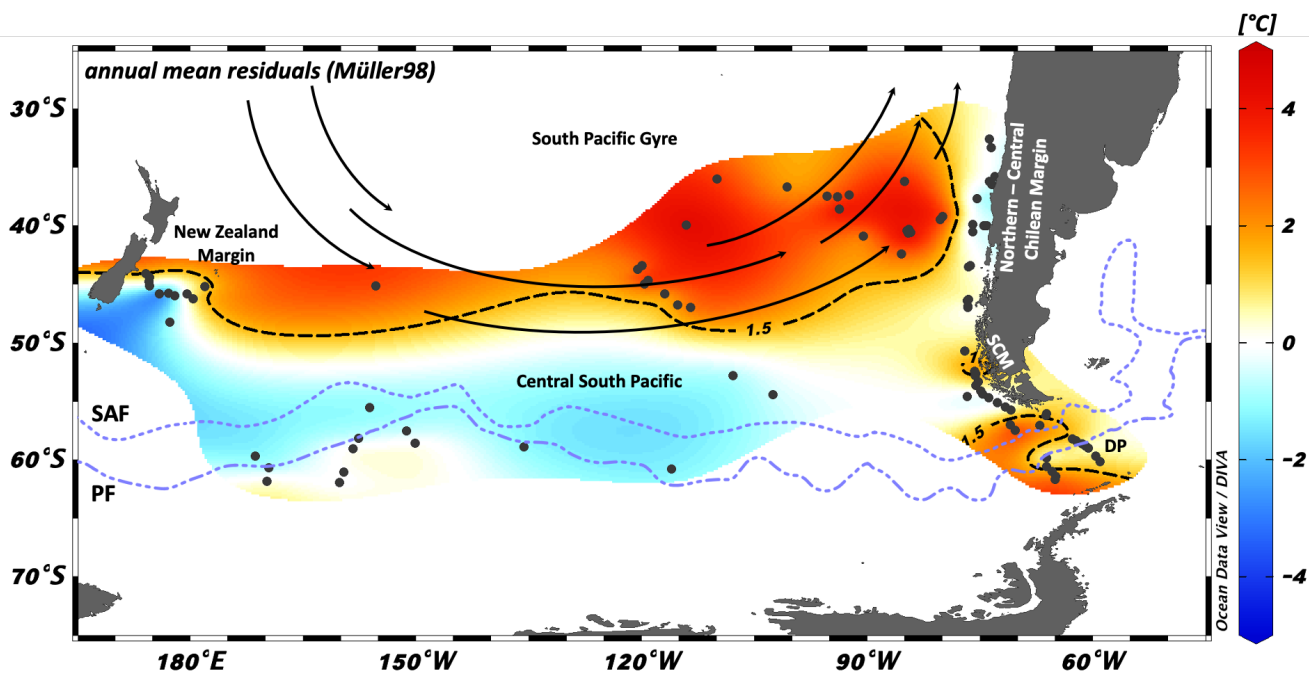
Figure 6: Map with residuals for the extended study area of the South Pacific with published data from the Central South Pacific, the New Zealand Margin, the South Pacific Gyre (Jaeschke et al., 2017) and the Chilean Margin (Prahl et al., 2006; this study; Prahl et al., 2010). Atlas-derived annual mean WOA05 water temperatures of 10 m water depth (Locarnini et al., 2006) were subtracted from the SST Müller98 calibration. SCM: Southern Chilean Margin; DP: Drake Passage; SAF: Subantarctic Front; PF: Polar Front.
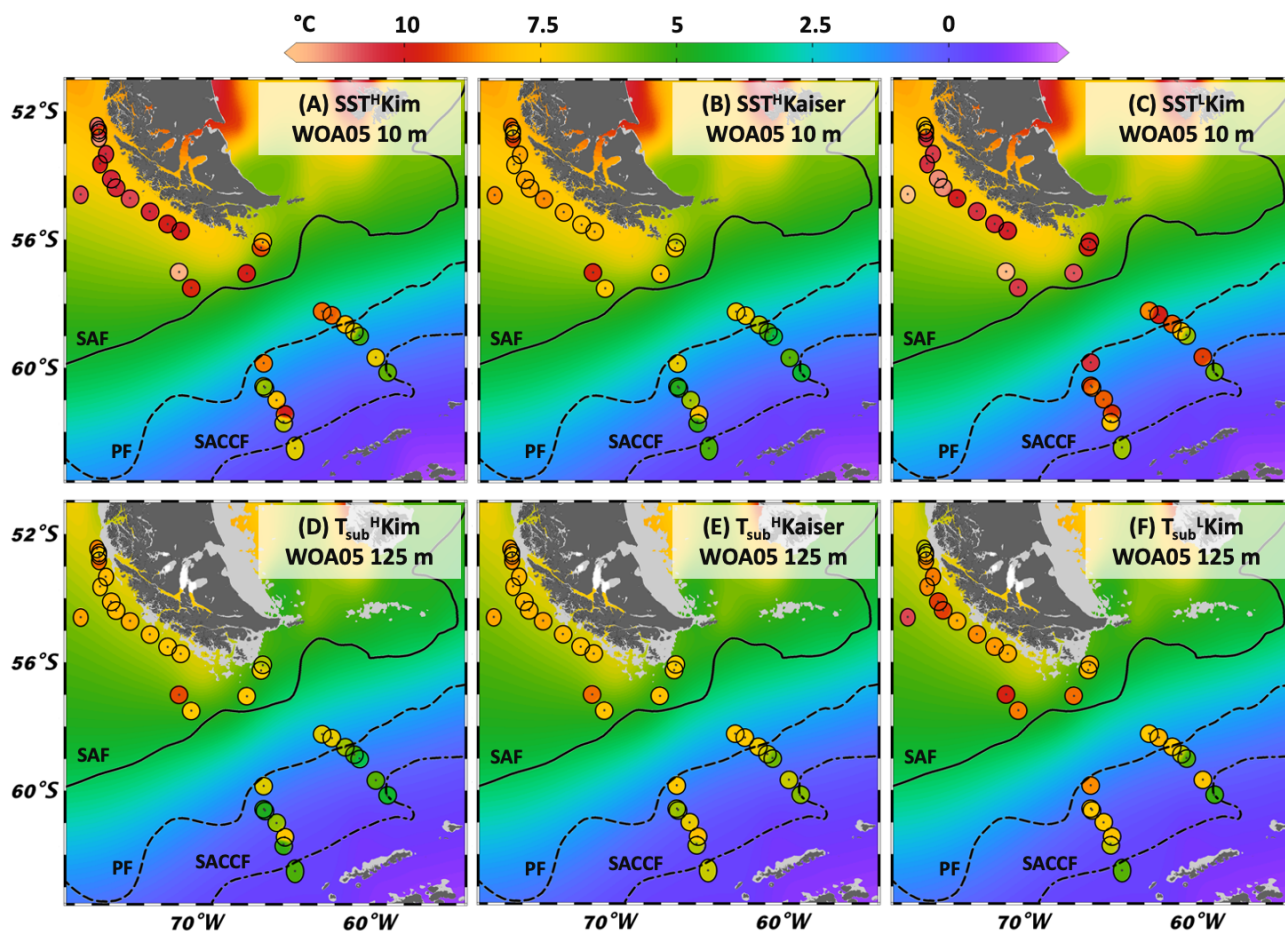
Figure 7: Map of reconstructed SST and Tsub values for TEX$^H_{86}$ and TEX$^L_{86}$ (this study). Background gridded annual mean temperatures at 10 or 125 m water depth: WOA05 data, colored dots are calculated SSTs or Tsub. (A) WOA05 SSTs with calculated data after SST^{H}Kim; (B) WOA05 SSTs with calculated data after SST^{H}Kaiser; (C) WOA05 SSTs with calculated data after SST^{L}Kim; (D) WOA05 Tsub with calculated data after Tsub^{H}Kim; (E) WOA05 Tsub with calculated data after Tsub^{H}Kaiser; (F) WOA05 Tsub with calculated data after Tsub^{L}Kim.
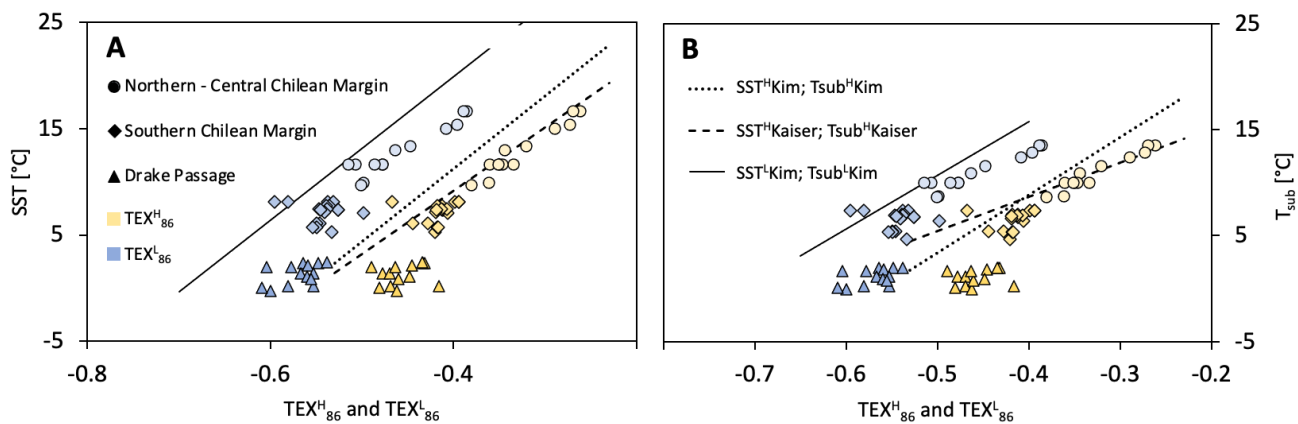
635

Figure 8: Comparison of TEX$^L_{86}$ (blue) and TEX$^H_{86}$ (yellow) data with water temperature with the SST 0 – 50 m water depth and Tsub 0 – 200 m (WOA05; Locarnini et al., 2006), respectively. Black line: TEX$^L_{86}$ calibration line (SST^{L}Kim, Tsub^{L}Kim) for surface and subsurface, respectively. Circles: Kaiser et al. (2015); Route: this study; triangle: Lamping et al. (2021) and this study.
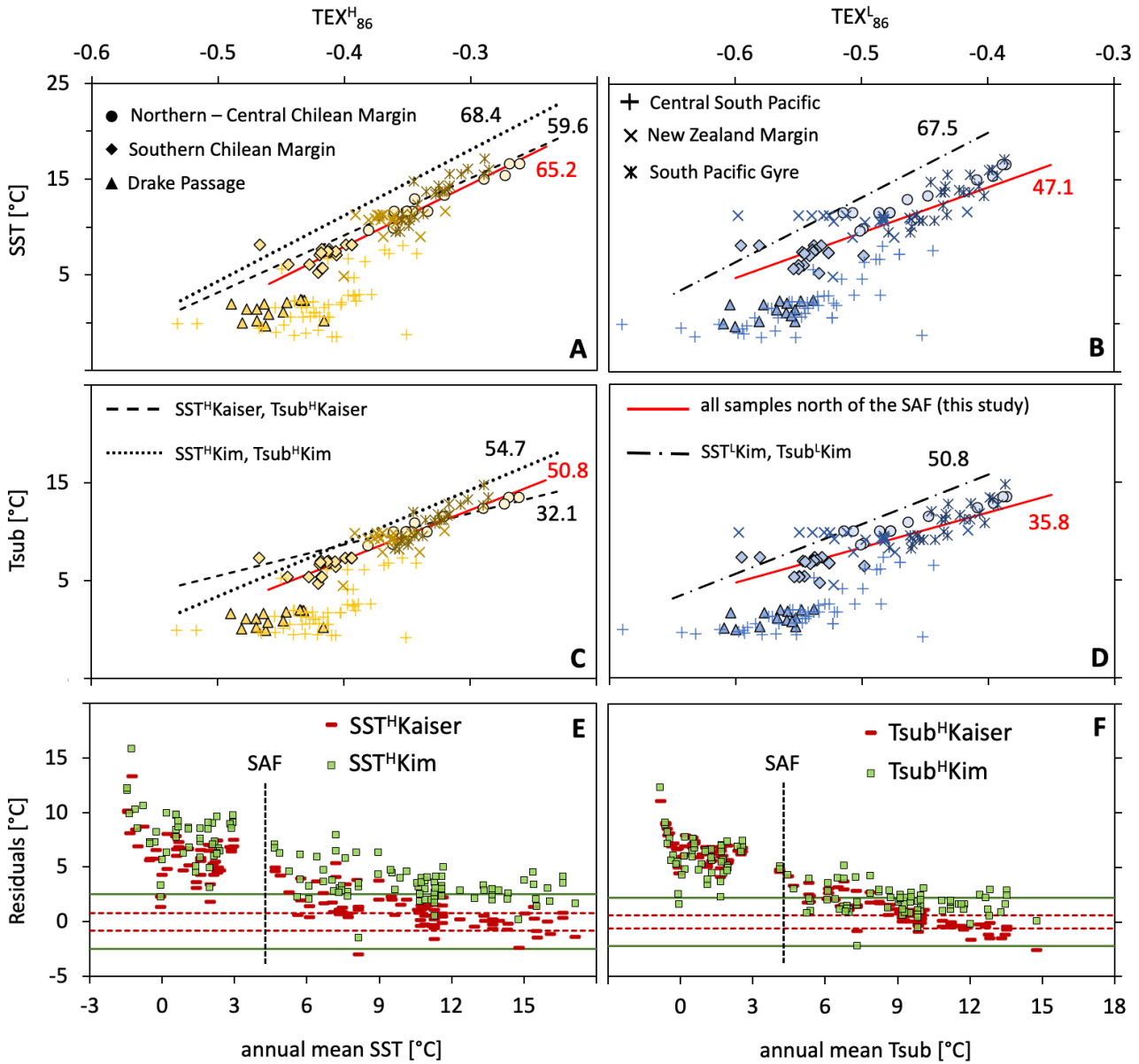
Figure 9: Comparison of TEX^H_{86} (yellow) and TEX^L_{86} (blue) data with annual mean water temperature with the SST $0 - 50$ m water depth and Tsub $0 - 200$ m (WOA05; Locarnini et al., 2006), respectively. The black (previous studies) and red numbers (this study) indicate the slope of the corresponding calibration. Central South Pacific, New Zealand Margin and South Pacific Gyre samples: Ho et al. (2014) and Jaeschke et al. (2017); Northern – Central Chilean Margin samples: Kaiser et al. (2015); Southern Chilean Margin and Drake Passage samples: Lamping et al. (2021) and this study. (E) – (F): Residuals for SST $0 - 50$ m and Tsub $0 - 200$ m, with modern world ocean atlas-based temperatures (WOA05; Locarnini et al., 2006) subtracted from the calibrated temperatures. Green solid lines: standard error of ±2.5° C (SST^HKim) and ±2.2° C ($Tsub^H$Kim). Red dashed lines: Calibration standard errors of ±0.8° C (SST^HKaiser) and ±0.6° C ($Tsub^H$Kaiser).
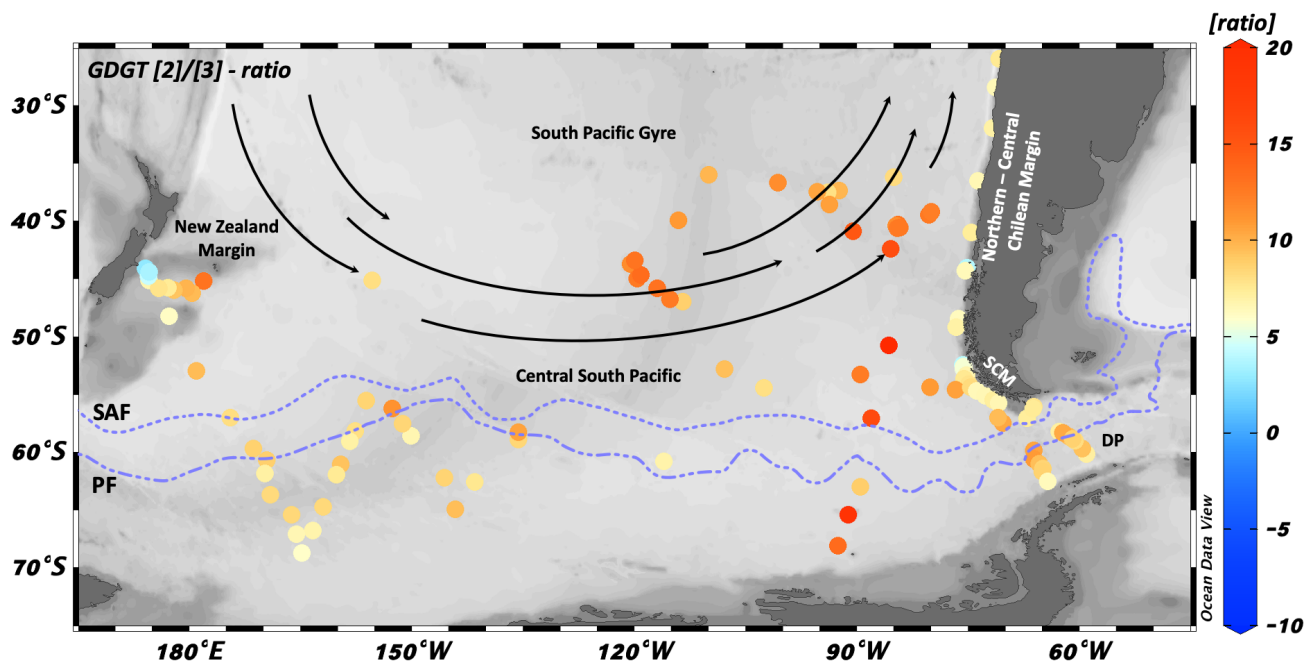
650

Figure 10: Map of GDGT [2]/[3]-ratios from our extended surface sediment sample set across different regions within the study area. SCM: Southern Chilean Margin; DP: Drake Passage; SAF: Subantarctic Front; PF: Polar Front.
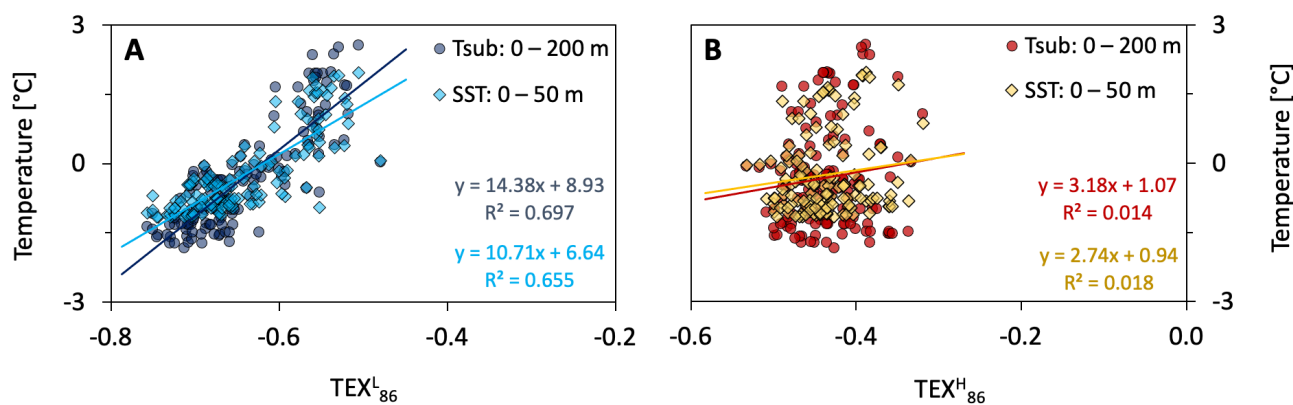
655 **Figure 11:** TEX$^H_{86}$ and TEX$^L_{86}$ Indices south of the SAF vs. modern WOA05 water temperatures. (A) TEX$^L_{86}$ of all South Pacific samples; (B) TEX$^H_{86}$ of all South Pacific samples.
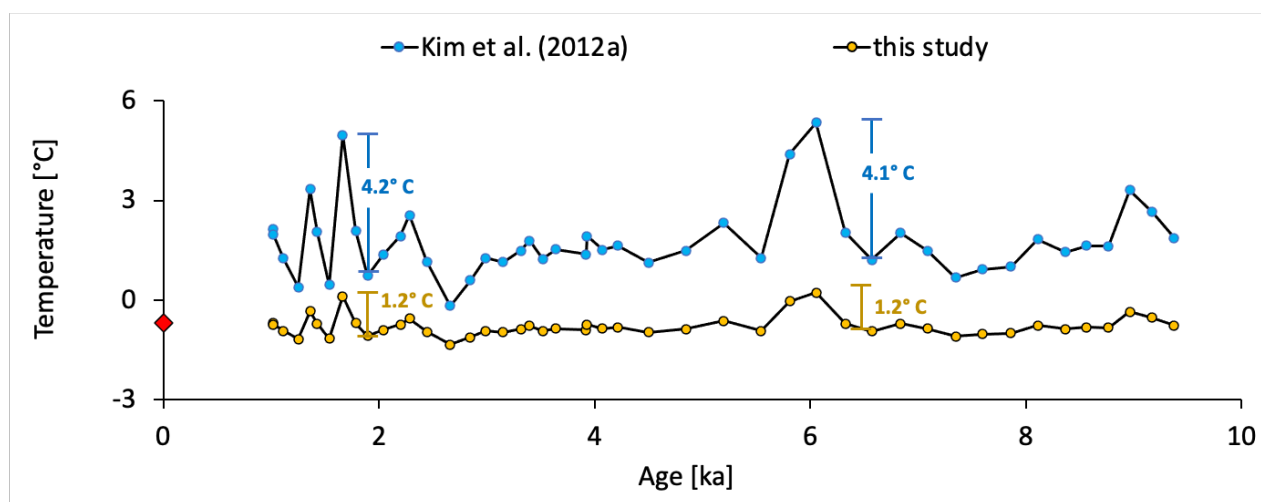
Figure 12: Comparison of core MD03-2601 (Kim et al., 2012b) with the temperature calibration Tsub^{L}Kim (blue) and the new subsurface calibration of this study (yellow). Red dot marked the mean temperature of 0 – 200 m water depth at the coring site.